Materials & Design 208 (2021) 109879

Contents lists available at ScienceDirect

Materials & Design

journal homepage: www.elsevier.com/locate/matdes

Modulation of virulence factors of *Staphylococcus aureus* by nanostructured surfaces

Paola San-Martin-Galindo [a,1,*], Emil Rosqvist [b,1,*], Stiina Tolvanen [b], Ilkka Miettinen [a], Kirsi Savijoki [a], Tuula A. Nyman [c], Adyary Fallarero [a], Jouko Peltonen [b]

[a] Drug Research Program, Division of Pharmaceutical Biosciences, Faculty of Pharmacy, University of Helsinki, Viikinkaari 5, 00014 Helsinki, Finland
[b] Physical Chemistry, Laboratory of Molecular Science and Engineering, Åbo Akademi University, Porthansgatan 3–5, FI-20500 Åbo, Finland
[c] Department of Immunology, Institute of Clinical Medicine, University of Oslo and Rikshospitalet Oslo, 0372 Oslo, Norway

HIGHLIGHTS

- Choice of the biofilm formation assay is crucial when designing functional surfaces.
- Use of multiple surface parameters enables comprehensive bacteria-surface analysis.
- Several topographical parameters correlate to phenotypic responses of *S. aureus*.
- Abundance profiles of several virulence proteins correlate to roughness parameters.

GRAPHICAL ABSTRACT

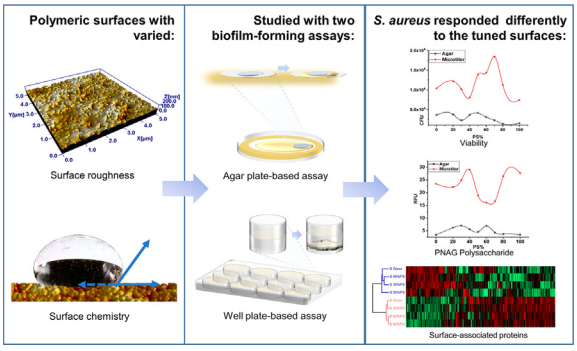

ARTICLE INFO

Article history:
Received 11 January 2021
Revised 26 April 2021
Accepted 6 June 2021
Available online 9 June 2021

Keywords:
Staphylococcus aureus
Biofilm formation assays
Surface proteins
Roughness
Physicochemical properties of surfaces
Surface chemistry

ABSTRACT

Investigating and understanding the response of microbes to various surfaces requires a versatile parametrisation of the surface, and multiple assays that captures the complexity of the biofilm structures. Here, *Staphylococcus aureus* biofilm viability, polysaccharide poly-N-acetylglucosamine, and proteins on the cell surface were analysed with agar plate- and well plate-based biofilm formation assays. Biofilms were grown on a set of nanostructured polymeric surfaces, which were thoroughly characterised for their surface chemistry and topography. Surface hydrophobicity, summit density as well as peak and valley structure were found to influence the microbial viability and exopolysaccharide abundance level in the agar plate assay. In the well plate assay, surface chemical parameters had a lesser influence on the viability, but roughness caused by valley structures increased the viability and decreased the exopolysaccharide expression. Surface proteins relating to pathogenicity were affected by the biofilm formation assay. The abundance profile of these proteins correlated clearly with several roughness parameters, especially fine structure parameters in the agar plate assay and lateral roughness in the well plate assay. These results highlight the necessity of describing the material surfaces with a versatile set of different roughness parameters to completely understand what specific features of a surface drive a certain bacterial response.

* Corresponding authors.
E-mail addresses: paola.sanmartingalindo@helsinki.fi (P. San-Martin-Galindo), emil.rosqvist@abo.fi (E. Rosqvist).
[1] These authors contributed equally to this work.

https://doi.org/10.1016/j.matdes.2021.109879
0264-1275/

1. Introduction

Bacterial attachment and biofilm formation are important processes in the understanding and counteracting of infections and fouling (e.g., in medical implants, water purification and food packaging) and they are key to understanding microbe-surface interactions. Bacterial motility, adhesion, sessile biofilm formation and dispersal are strategic responses to environmental conditions including surface properties, nutrient density and shear forces [1,2].

The formation of bacterial biofilms is a dynamic process that confers tolerance to antibiotics and disinfectants, while enhancing host colonisation and facilitating immune evasion. In particular, *Staphylococcus aureus* is recognised as one of the most frequent pathogen of nosocomial infections. Biofilms formed by *S. aureus* are associated with multiple chronic wound infections (e.g., venous leg ulcers, burn wound colonisation), as well as medical device implants colonisation (e.g., heart valves, orthopaedic devices, penile prostheses) [3,4]. The propensity of bacterial biofilm attachment to a surface depends on environmental and experimental conditions [5–7]. The adhesion process begins when bacteria approach a substrate surface. During the approach they adopt sensing mechanisms to detect beneficial areas to which to adhere, based on the surface's physical and chemical character, such as surface charge, stiffness and topography [8–10]. The bacteria may adapt to the sensed surface by altering their own properties (e.g., cell surface charge, size and shape), or by directly interacting with the surface (e.g., via ion and/or molecule trapping) [8]. In some cases, the bacteria are not attached directly onto the surface, but rather to a conditioning film of excreted exopolymeric substances. The initial adherence of even a limited population of adherent microbes can stimulate the adhesion of others and allow for the attached bacteria to replicate and colonise the surface [1]. Surface sensing may also trigger an upregulation of virulence factors [11].

Bacterial attachment begins with reversible adhesion, which eventually becomes irreversible due to the excretion of polysaccharides, proteins, and extracellular DNA, among others, which are constituents of the biofilm matrix [1,8,10]. The exopolysaccharide poly-N-acetyl-β-(1,6)-glucosamine (PNAG) is a positively charged carbohydrate net that constitutes largely to the *S. aureus* biomatrix. PNAG facilitates the cell–cell adhesion that eventually leads to biofilm formation [12–14]. Proteins in the biomatrix are self-secreted via numerous mechanisms that they have developed in response to environmental determinants and surface attachment [15,16]. Cell wall-anchored proteins (CWP) and proteins secreted to the extracellular milieu are of particular interest as they are generally considered as important determinants of *S. aureus* pathogenesis [15].

Numerical and analytical methods like surface element integration (SEI) and Derjaguin's integration have been used to incorporate topographical effects to (substrate surface)-(colloidal particle) interactions as predicted by the Derjaguin-Landau-Verwey-Overbeek (DLVO) theory for colloidal stability of the initial adhesion [8,9,17]. The results have indicated that textured surfaces have a lower interaction energy compared to smooth counterparts during the initial bacterial attachment. These approaches are in line with observations of an association of physical heterogeneity with improved microbial adhesion of certain Gram-positive and Gram-negative bacteria species [17]. The approach of tuning surface chemistry and topography, thereby affecting the thermodynamics of adhesion, is motivated in order to understand, and ultimately control, microbial adhesion to a surface of materials of interest [1,18,19].

The complex bacteria-surface interactions, occurring through the medium, and differences between bacterial species, make it difficult to decouple different factors in the adsorption process [8,20]. Several reports have highlighted a length-scale dependence of the response to roughness, especially where surface features are proportional to the size of the bacterium [8,21,22]. Different roughness parameters and length scales have been used in different studies, which makes a proper comparison challenging. The use of several roughness parameters for describing a surface geometry accurately is commendable, as vastly different surface structures can share a similarity in some parameters. In addition to the commonly used average roughness (S_a) or RMS-roughness (root mean square, S_q) for depicting height variations, parameters that describe other properties of a surface should be utilised. These are, among others, effective surface area, summit density, correlation lengths, and functional surface parameters such as peak heights and valley depths [23].

Various publications have suggested roughness as being only a minor factor after initial adhesion, while others have reported marked effects of roughness as well as surface energetics on bacterial cells [24–27]. Interestingly the bacterial response has been observed to correlate to nanoscale differences [28,29], but *S. aureus* has also shown a preference to surfaces with regular, larger features [28].

Several studies discussing biofilm formation on substrates with varying or tuned surface properties have focused only on quantifying the attachment by the traditional counting of colony units, which fails to capture the complexity of the biofilm structures [30,31]. By contrast, the aim of this study was to understand, in-depth, the *S. aureus* biofilm dynamics on nanostructured substrates with controllable surface chemistry and topography, as well as to clarify the role of physicochemical factors that influence bacterial colonisation.

Nanostructured surfaces can be prepared by coating a substrate with a blend of two lattices. The nanostructure arises from the different properties of the latex components. One of the components is a film-forming low-T_g latex (e.g., acrylonitrile butadiene styrene, ABS) while the other, high-T_g component (e.g., polystyrene, PS) remains as particles in the coated film. The nanostructure can be adjusted through varying mixing ratio of the latex components. Also, the particle size (particularly of the high-T_g component) influences the coating structure. We have previously used such nanostructured surfaces to modulate the growth of human dermal fibroblast [32], to support ARPE-19 cells (human retinal pigment epithelial cells) [33] and to preliminarily test adhesion of proteins and *S. aureus* [34]. The highly processable latex blend coatings have also been applied for preparing a paper-based test platform for mammalian cell and biofilm studies [35]. Being inspired by the promising test results, we report here a detailed study on how the nanostructured latex film influences the response of the bacterial colonisation and biofilm formation

Due to the varying responsiveness of bacterial growth to external conditions, the biofilm formation of *S. aureus* was compared using two of the most common static biofilm formation assays for surfaces studies in laboratory settings: an agar plate (AP)-based and a well plate (WP)-based biofilm formation assay. Together with the set of polymeric surfaces, the effect of both the physico-chemical material surface properties and the environmental conditions on the biofilm development were simultaneously analysed. The surface properties (wetting, surface chemistry, and roughness) were thoroughly characterised and the bacterial responses on them were investigated. Understanding variations in cell viability, PNAG abundance, and surface proteins on various surfaces can contribute to tailored design and engineer-

ing of biomaterials as well as medical devices in the long term, for which bacterial adhesion and colonisation susceptibility can be effectively controlled.

2. Materials and methods

2.1. Materials

2.1.1. Latex surfaces

Two different aqueous latex dispersions were used in this study — a dispersion of polystyrene (PS) particles (HPY83, Styron Europe GmbH, CH) with an average particle size of 130 nm and a glass transition temperature of 105 °C as reported by the manufacturer, and a dispersion of acrylonitrile butadiene styrene (ABS) copolymer particles (HPC26, DOW Europe GmbH, CH) with an average particle size of 140 nm and a glass transition temperature (T_g) of 8–10 °C as reported by the manufacturer.

2.2. Instrumental

2.2.1. Atomic force microscopy

The surface topography was imaged by using a Nanoscope V MultiMode 8 atomic force microscope (AFM; Bruker, USA). Images captured were of 5 μm by 5 μm size with a 512 by 512 pixels resolution. Silicon cantilevers with a nominal tip radius of curvature of 10 nm (NSG01, NT-MDT, Russia) were used for imaging.

The image analysis software Scanning Probe Image Processor (SPIP; Image Metrology, Denmark) was used for image preparation and calculating the surface roughness parameter values (Fig. S1a-c). Gaussian filtering (ISO 11562) of the captured topographs of the latex surfaces was conducted with the software. A 0-th degree LMS fit was also applied when necessary. Descriptions of the used roughness parameters can be found in the supplementary material.

2.2.2. Contact angle measurements and surface energy determination

Equilibrium contact angles were determined on washed and dried latex films with a CAM200 goniometer (KSV Instruments Ltd, Finland). Droplets of 2 μL volume (1.4 μL for DIM) were dispensed on the surface and the contact angle was recorded for 20 s. Three probe liquids were used for calculating the surface energy: Milli-Q water, diiodomethane (DIM), and ethylene glycol (EG). The contact angles were determined with a software supplied with the instrument, which uses a Young-Laplace fitting method to the drop silhouette curvature.

The measured apparent water contact angles were corrected for roughness using the Wenzel equation [36]:

$$cos\theta_A = r \cdot cos\theta_Y,$$

where θ_A is the apparent contact angle, θ_Y Young's contact angle and r is the roughness factor. The roughness factor r was calculated from the developed surface area data as $r = \left(1 + \frac{S_{dr}}{100}\right)$ [37].

Surface energies were calculated with the Owens-Wendt-Rabel-Kubelka (OWRK), van Oss-Chaudhury-Good and Kaelble methods, respectively. The used surface tension values of the probe liquids were those suggested by van Oss-Chaudhury-Good [38].

2.3. Methods

2.3.1. Manufacturing of the surfaces

The ABS and PS latex dispersions were mixed in volume ratios 80:20, 70:30, 60:40, 50:50, 40:60, 30:70, and 20:80. The blend ratio is hereafter given as the relative content of the PS dispersion in the surface film. These latex blends, as well as pure PS and ABS dispersions, were further diluted in a 1:3 ratio with Milli-Q water for ease of processing. The coatings were made by drop casting approx. 20 μL the blend onto glass coverslips (VWR International, LLC, USA) with a 13 mm diameter, after the coverslips had been rinsed with water and ethanol, and plasma-cleaned for 5 min. It has been shown that an IR treatment and washing removes biocides and additives from the outmost latex surface [39]. After 1 h of drying at room temperature (RT), the coated coverslips were IR-treated and finally oven-dried (1 h in 105 °C). More details on the manufacturing can be found in [32].

2.3.2. S. aureus culture conditions

Routinely, an inoculation loop of a pure *S. aureus* ATCC 25923 culture stock was streaked onto a tryptic soy agar (TSA; Neogen®, Lansing, Michigan, USA) plate and incubated at 37 °C for 18 h. The bacterial culture was obtained by transferring single colonies of *S. aureus* into 100 mL of tryptic soy broth (TSB; Neogen®, Lansing, Michigan, USA), which was then incubated in aerobic conditions for 16–18 h (220 rpm, 37 °C) until bacterial growth reached 10^8 colony-forming units (CFU) per mL. This was verified by measuring the optical density at 595 nm with a Multiskan Sky Microplate Spectrophotometer (Thermo Scientific, Vantaa, Finland), followed by viable cell counting on TSA plates.

2.3.3. S. aureus biofilm formation using two static biofilm assays

In the AP-based assay, the colonisation of *S. aureus* onto the latex surfaces was conducted as recently reported [40]. Briefly, 1.5 mL of bacterial suspension (1:10 dilution of the bacteria culture in TSB, which estimated 10^7 CFU/mL) was spread evenly over a sterile Whatman filter paper (70 mm diameter, qualitative grade 2, GE Healthcare, Little Chalfont, UK) on a TSA plate (100x17mm dish, Nunclon™ Delta). Subsequently, latex surfaces were sterilised (10 min exposure to absolute ethanol followed by air drying) and placed on top of the filter paper with the coating side facing downward. This assembly was incubated under humidified conditions at 37 °C for24 h. In the WP-based assay, sterile latex surfaces (sterilised as described above) were first placed (coating side facing upward) on flat-bottomed 12-well plates (Nunclon™Δsurface, Thermo Scientific, Roskilde, Denmark), followed by the addition of 1.5 mL of the *S. aureus* bacterial suspension (estimated 10^7 CFU/ml). The bacteria were grown for 24 h, at 37 °C, under aerobic conditioning with shaking (220 rpm).

Each latex blend surface (0–100% PS) (prepared as described in Section 2.3.1) was assessed in two biological repetitions with three technical replicates in every biofilm quantification assay. Uncoated glass coverslips were used as material surface controls.

2.3.4. Quantification of S. aureus biofilm growth by viable cell count

Once the biofilms were grown onto the latex surfaces as described above, the 24-h biofilms were dislodged by a combination of vortexing and sonication [40]. The sample surfaces were dipped into fresh TSB to remove non-adherent cells, and then transferred to 1 mL of sterile solution Tween® 20-TSB at 0.5% (w/v) in a 50 mL conical tube. The tubes were vortexed twice for 10 s, with sonication in between during 5 min (at 25 °C, 35 kHz) in a water bath (Ultrasonic Cleaner 3800, Branson Ultrasonics, Danbury, CT, USA). Afterwards, the bacterial solution was subjected to 10-fold serial dilutions using TSB and plated on TSA plates. After 18 h of incubation at 37 °C, viable colonies were counted. The bacterial growth on each sample surface was expressed as an average of CFU per cm^2.

2.3.5. Quantification of S. aureus biofilm matrix through the poly-N-acetyl-β-(1,6)-glucosamine (PNAG) fraction

The quantification of the PNAG fraction was performed using Wheat Germ Agglutinin Alexa Fluor® 488 conjugate (WGA; Molecular Probes Inc., Eugene, OR, USA). The previously described protocol by Skogman et al. was applied with some modifications [41].

The biofilms already formed onto the latex surfaces were soaked once in sterile phosphate buffered saline (PBS) to get rid of loose cells and then placed coating side facing upward into a 24-well plate. A 15 μg/mL WGA-staining solution was added into each well followed by an incubation at 4 °C in darkness. After 2 h of dye fixation, the samples were washed thrice with PBS and let air-dry at room temperature. The latex surfaces were then transferred to 50 mL conical tubes containing 1 mL of 33% acetic acid, sonicated for 30 s (25 °C, 35 kHz), incubated at 37 °C during 1 h, and sonicated once again for 30 s. Lastly, an aliquot of 200 μL of the remaining suspension was transferred to 96-well plates for measuring the fluorescence signal ($\lambda_{excit.}$ = 495 nm; $\lambda_{emis,}$ = 520 nm) using Varioskan™ LUX Multimode Microplate Reader (Thermo Scientific, Vantaa, Finland). The fluorescence signals were blank-corrected for each latex blend surface.

2.3.6. Trypsin-shaving of S. aureus biofilms and measurement of protein concentrations

For trypsin shaving, 24-h biofilms were grown in triplicate on the latex blends (30%, 50%, 60% PS) and on the bare glass coverslip using both static biofilm assays as described above (Section 2.3.3). A previously published trypsin-shaving method for proteomic studies [42] was optimised in terms of trypsin concentration and incubation treatment. The suitability of the optimised trypsin-shaving method for maintaining the cell integrity was corroborated by viable cell count of the harvested cells after incubation with and without trypsin. A brief description of the protocol is described in the supplementary material.

2.3.7. Identification of trypsin-released proteins/peptides by LC–MS/MS

The peptide samples were analysed with LC-MS/MS as reported previously [43,44]. A brief description of the protocol is described in the supplementary material. The mass spectrometry proteomics data have been deposited into the ProteomeXchange Consortium via the PRIDE partner repository (dataset identifier PXD022301) [45].

2.4. Data processing and statistical analysis

Surface roughness parameter errors are given as a 99% confidence interval (CI), whereas the surface chemistry data was presented with the standard deviation. Coefficients of determination were obtained by Origin (Origin2020, Version Number 9.7.0.188. OriginLab Corporation, Northampton, MA, USA).

Statistically significant differences ($p < 0.05$) in the quantification of bacterial colonisation (number of viable cells and PNAG-fraction), among the latex surfaces of each biofilm formation assay, were determined by Brown-Forsythe analysis of variance (ANOVA) followed by Tamhane's T2 post-hoc test. Student *t*-test with Welch's correction was used for comparing a single material between assays. Both calculations were performed using GraphPad Prism software (version 8.0.0). The repeatability of the two static biofilm assays was assessed using the standard deviations for all the means, while the Coefficient of Variations (CV) of the control biofilms were calculated by ratio of the repeatability standard deviation and the average measurement [46].

For label-free quantitative analysis of the proteome data, missing LFQ values were imputed by random draws from a low abundance-adjusted distribution, followed by normalisation of the relative abundances of proteins using Z-score by the Perseus software (version 1.6.5.0). Protein intensities were transformed to be expressed logarithmically (base 2), and only proteins expressed in at least 2 out of 3 replicates were considered valid protein identifications. In the analysis of differential expression within each biofilm-forming assay, a multiple comparison analysis (ANOVA) was also performed in the Perseus software, where three replicates per sample were used based on their $\log_2$-transformed LFQ abundances. A permutation-based false discovery rate of 0.1 was applied in this exploratory analysis of significant difference among the samples. The STRING database (version 11.0) was used for studying protein interactions and functional enrichment analysis (FDR < 0.05) [47]. Protein correlation strength was evaluated with R-squared and adjusted R-squared obtained from curve fitting with the Origin software. Additionally, Pearson's chi-squared test and Student's *t*-test were determined for the correlations (cut-off value for Pearson's *r* was set at |0.8|).

3. Results

3.1. Surface characterisation

3.1.1. Surface roughness characterisation of the coatings

The topography of the surfaces was characterised thoroughly with AFM. A set of roughness parameter values is collected in the Table S1a and S1b, including Fig. S2a–f. Here, key descriptive figures of the topography and roughness are introduced to illustrate the structural differences between the studied surfaces.

The pure ABS film (0% PS) appeared as the smoothest surface, being logical for the low-T_g film forming latex component (Fig. S3). Introduction of PS made the surface rougher and maximum roughness was observed at 50% (e.g., S_q) to 60% PS (e.g., S_{dr}, S_{bi}, S_v), depending on the roughness parameter in question (Fig. 1a). The topography on either side of this maximum was not entirely similar, however. Introduction of PS and increasing its content increased roughness predominantly caused by an increasing number of local maxima, i.e., the PS spheres (high-T_g latex), on the surface. In the reverse case, i.e., going from a 100% PS film to lower PS contents, through increasing number of valleys between the annealed PS particles. The use of a set of different roughness parameters allows for an intriguing parameter-decoupling analysis in search of correlations between roughness and microbial culture.

3.1.2. Surface chemical characterisation of the coatings

The surface chemistry and wetting characteristics of the surfaces were determined with contact angle goniometry (Table 1). Using the contact angle data, corrected for the roughness data described in Table S1a and 1b, the surface chemistry was determined using the van Oss-Chaudhury-Good (VCG) model. These results are presented in Table S1a and 1b. The water contact angle was observed to be around 72°–76° for the films with 0–60% PS, increasing slightly for 80% PS, and finally, for the pure PS film, getting least hydrophilic with a contact angle of 90.2°.

Fig. 1b illustrates the changes in surface energy and its components as a function of PS content. The total surface energy and the dispersive component was determined to be within 42–44.6 mJ/m^2 for the high and low PS blends. In the mid-range, 40% and 60% PS, both parameters decreased by about 5 mJ/m^2. These surfaces were also the roughest and the reduction of surface energy is probably due to a reduction in the Lifshitz-van der Waals interactions because of increased topographic heterogeneity. The polar negative component of surface energy was at a level of 10–11 mJ/m^2 for the films 0–60% PS, then decreasing for the 80% PS and was finally reaching the minimum of 0.7 mJ/m^2 for the 100% PS surface. For the whole series, the polar positive component was negligible. Together with the water contact angle data, the reduction in polar negativity for high-PS surfaces indicates that a thin layer of ABS covered the surfaces up until 60% PS, beyond which progressively more PS regions were exposed. It should be noted that contact angle measurements are macroscopic scale measurements for

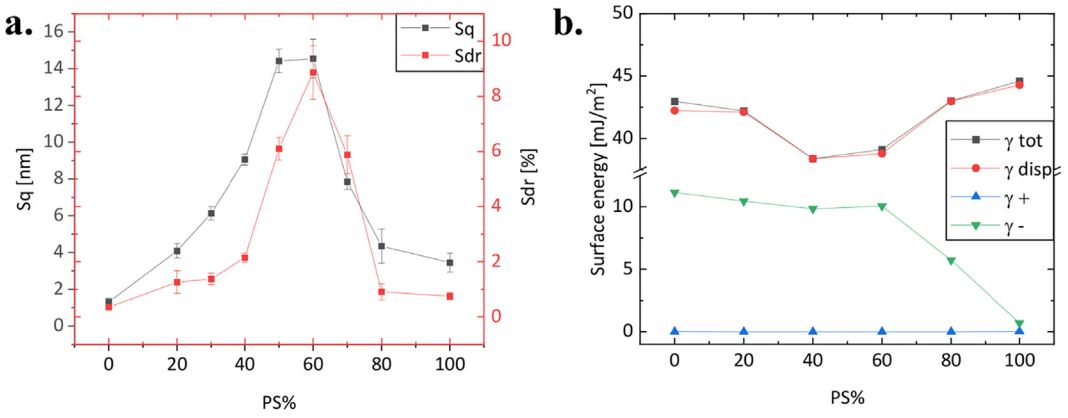

Fig. 1. (a) Roughness variations in terms of RMS roughness, S_q, (black) and effective surface area, S_{dr}, (red) in relation to the polystyrene content in the surface films. Error bar shown is the 99% confidence interval (CI). (b) Surface energy as a function of PS content in the latex films determined from contact angle data according to the VCG model. Black indicates the total surface energy (γ_{tot}), red the dispersive surface energy (γ_{disp}), and blue and green the negative respectively positive polar contributions (γ_+) and (γ_-) to the surface energy. (For interpretation of the references to colour in this figure legend, the reader is referred to the web version of this article.)

Table 1
Water (MilliQ), ethylene glycol (EG), and diiodomethane (DIM) contact angle data as a function of the polystyrene content of the surfaces, and surface energies determined therein. Contact angles (CA) have been corrected for roughness. Error given is the standard deviation.

Surface (% PS)	Water CA [°]	EG CA [°]	DIM CA [°]	γ^{tot} [mJ/m²]	γ^{disp} [mJ/m²]	$\gamma^{pol(-)}$ [mJ/m²]	$\gamma^{pol(+)}$ [mJ/m²]
0	71.8 ± 4.1	38.6 ± 9.4	34.3 ± 5.6	43.0	42.2	11.1	0.0
20	73.4 ± 3.4	41.9 ± 7.1	33.9 ± 7.8	42.2	42.1	10.4	0.0
40	76.3 ± 6.6	46.9 ± 9.4	40.4 ± 8.4	38.4	38.4	9.8	0.0
60	74.5 ± 6.7	41.8 ± 8.7	35.8 ± 5.0	39.1	38.8	10.1	0.0
80	79.9 ± 3.5	44.4 ± 10.2	31.7 ± 6.4	43.0	43.0	5.7	0.0
100	90.2 ± 16.2	45.7 ± 21.4	29.3 ± 11.5	44.6	44.3	0.7	0.0

which local non-ABS-covered regions in low-PS surfaces might be indiscernible.

3.2. Bacterial response

3.2.1. Comparison of biofilm-forming conditions between the static biofilm assays

Several aspects of the conditions of two biofilm growth assays were calculated considering bare glass coverslip as the control surface. As shown in Table 2, similar values of logarithmic biofilm growth and planktonic inoculum density were observed for both experimental systems. Similarly, there were no substantial differences in the measurements of repeatability standard deviation as well as coefficient of variation. More importantly, these values were low, thereby indicating reliability among the repetitions. The only noticeable difference between these biofilm assays was found in the surface-area-to-volume ratio (more than 15-fold), which might be a key factor that causes changes in the microenvironment of *S. aureus*, and thereby influences the biofilm colonisation and formation. A closer examination of the differences in the bacteria colonisation levels is presented in the following sections.

In the AP-based assay, the bacterial colonisation was higher when PS was the minor component, with 30% PS being an exception. When PS became the dominant component, bacterial colonisation decreased, reaching the minimum for surfaces with 80–100% PS, being on the same level as the glass control. In the WP-based assay, the maximum bacterial colonisation was observed within 50–70% PS, while the lowest one was observed at 100% PS (Fig. 2a). Comparisons between the two assays showed that the 70% and 80% PS surfaces were the most influenced by the biofilm formation conditions since bacterial colonisation levels were over eight times higher when using the WP-based assay compared to the AP-based assay (Fig. S4a). Also, the surface 60% PS displayed the greatest significant difference between the biofilm growth assays.

In a closer examination of the bacterial colonisation within each biofilm assay, statistically significant differences between the latex surfaces were found only in the AP-based assay. The 0% PS promoted a statistically higher number of CFUs per cm^2 than the high PS surfaces (80% and 100% PS) (Fig. 2a). Additionally, for this growth condition, there was overall smaller variations between repetitions.

3.2.2. Variation in the bacterial colonisation level in different surface chemistry conditions and biofilm-forming assays

The viability of 24-h *S. aureus* biofilms on the latex surfaces was first measured in terms of attached viable counts (colony-forming units, CFUs) on the two different biofilm growth assays. Notably, the density of viable cells adhered to all the surfaces (latex-coated surfaces and bare glass) was higher in the WP-based assay (Fig. 2a). This may relate to its low surface-area-to-volume ratio, conditions in which the bacterial cells as well as the nutrient broth may be forced to concentrate in a reduced area.

3.2.3. Variations in the PNAG-fraction abundance on different surfaces and in different biofilm-forming assays

The production of the exopolysaccharide PNAG during the biofilm formation process causes an irreversible bacterial attachment, which leads to bacterial accumulation. This component (PNAG) has been shown to play a key role in maintaining the biofilm structure and the integrity of the microbial community within the biofilm [13,14]. In this part of the study, the propensity of the bacteria to produce PNAG onto the latex surfaces was investigated in the two static biofilm assays.

Table 2
Comparison of biofilm-forming conditions in the two static assays to the control surface (glass).

	Calculated surface-area-to-volume (SA/V) ratio	Control biofilm (log_{10} CFU/cm^2) mean ± SD	Planktonic inoculum (log_{10} CFU/mL) mean ± SD	Repeatability Standard deviation (SD)	Coefficient of variation (CV) (%)
AP-based assay	37.80 cm^{-1}	5.14 ± 0.18 n = 6	8.57 ± 0.15 n = 6	0.18	3.5
WP-based assay	2.33 cm^{-1}	5.79 ± 0.24 n = 6	8.54 ± 0.11 n = 6	0.24	4.1

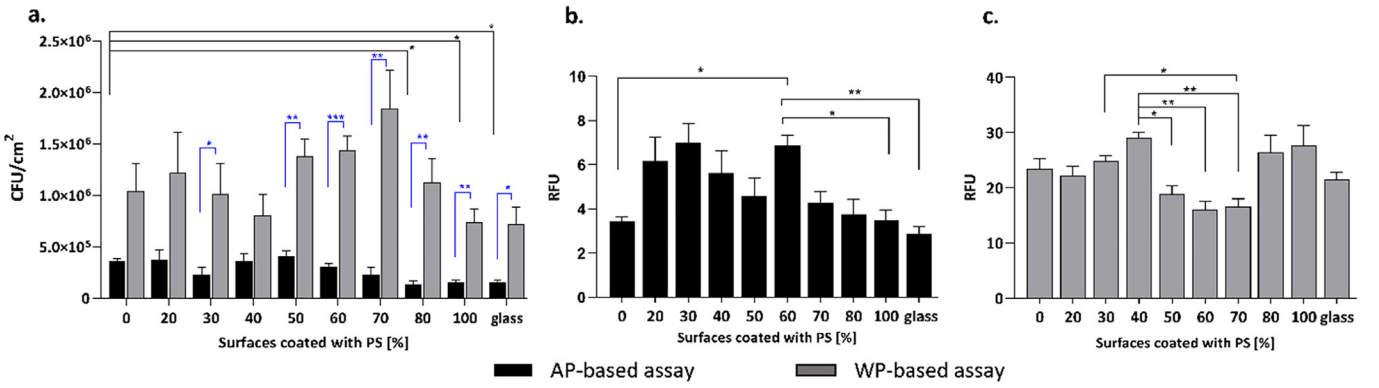

Fig. 2. Quantification of 24-h *S. aureus* biofilms in terms of (a) viable cell counts, and (b, c) PNAG on the set of modified surfaces in two biofilm-forming assays. Bacterial colonisation is represented in CFUs per cm^2, whereas the PNAG-fraction is in relation to relative fluorescence units (RFU). Brown-Forsythe ANOVA followed by Tamhane's T2 post-hoc for multiple comparisons was used to determine statistical differences within each biofilm formation assay, while Student *t*-test with Welch's correction was used for a single material between assays. * indicates $p < 0.05$; ** $p < 0.01$; *** $p < 0.001$. Error bars show the standard error of the mean (SEM) of two biological repetitions with three technical replicates. Note that 0% PS surface indicates a coating purely with ABS.

In the AP assay, the most significant observation was the low detected amount of PNAG on the smoothest surfaces (0%, 80%, and 100% as well as glass). The detection of a higher fluorescence signal associated to PNAG was observed on surfaces with 20–60% PS, with 50% PS being an exception (Fig. 2b). Indeed, the 60% PS surface was a unique surface in that it showed significantly higher amount of PNAG under this assay condition, having the biggest difference to the glass surface (Fig. 2b).

In the WP assay, the lowest fluorescent signal (specific to PNAG) was detected in biofilms formed on the surfaces with 50–70% PS, being even slightly below the level of the reference glass substrate (Fig. 2c). The other latex surfaces showed a higher fluorescence signal than that of the glass surface, with the maximum signal detected on 40% PS. Additionally, more frequent statistical differences in the fluorescence signal for this polysaccharide were observed in contrast to the few statistical differences among the surfaces in terms of CFU per cm^2.

The lowest variations in PNAG abundance (ratio below 0.4), as measured by the specific fluorescence signal, between the two assays, were observed on the 60% PS surface, i.e., the roughest surface (Fig. S4b). An opposite effect occurred with the smoothest surfaces (0%, 80% and 100% PS), including the glass surface, which all showed variation ratios above 0.8 (Fig. S4b). This indicates that experiments done on the flat surfaces were more influenced by the biofilm growth assay. When using the WP assay, the quantified *S. aureus* PNAG fluorescent signal on the surfaces was higher. Interestingly, the biofilm-forming assays showed almost the opposite trends with the lowest detected PNAG signal on the roughest surfaces (50–70% PS) in the WP assay, and the flatter surfaces (20–40% PS) showed a higher PNAG fluorescence signal in the AP assay.

3.2.4. Associating number of viable cells and PNAG amounts of S. aureus biofilms on different surfaces

To assess the biofilm colonisation onto the latex surfaces in terms of viable counts and matrix-associated PNAG, these parameters were plotted by surface type (Fig. S5). In the AP assay, the latex surfaces seemed to be divided into four groups. The high PS surfaces (70–100% PS) appeared to give low CFUs and PNAG production, while the very flat 0% PS surface and the relatively rough 50% PS surface were associated with a high biofilm density and low biomatrix production. On the opposite section (Fig. S5), while 30% PS surface and, to a lesser degree, the 60% PS caused high PNAG amounts for the number of colonies present on the surface, the 40% and 20% PS as well as the glass surface displayed average ratios of CFU to PNAG-specific fluorescence signal (RFU).

The associations of PNAG-component biomatrix with the number of *S. aureus* viable cells in the WP assay were rather different. Here, the PNAG content seemed to decrease as the biofilm density increased (Fig. S5). Biofilms on the glass seemed to have a slightly lower PNAG fluorescent signal, when compared to latices with similar biofilm density (40% and 100% PS). The trend also had subgroupings with the non-polar surfaces (80% and 100% PS) yielding some of the highest PNAG contents. The rougher surfaces (apart from the 40% PS) all showed higher amounts of CFU with lesser biomatrix expression. The roughest surfaces, 50% and 60%, showed the highest number of colonies and lowest PNAG signal. Some topographical aspects of these surfaces were similar – in particular, the S_q roughness values, being 14.4 nm and 14.5 nm for the 50% and 60% PS samples, respectively. The S_q value of the 30% PS was 6.1 nm, and 7.9 nm for the 70% PS, the range being 1.3–14.5 nm for the full series. This latter pair also showed some resemblance to each other, for instance with respect to the core valley depth, which was 12.9 nm and 14.1 nm (range 2.1–26.2 nm) for the 30% and 70% PS surfaces, respectively. The 50–70% PS surfaces also had the highest S_{dr} values of the series, at 6.1%, 8.9%, and 5.9% respectively, meaning that the lowest biomatrix expression was observed on the surfaces with highest effective surface area.

Taken together, this outcome reinforces the role of the biofilm growth conditions (in this study represented by AP- and WP-based assays) on the PNAG abundance of biofilms formed on different surfaces.

3.2.5. Comparison of S. aureus surfaceome profiles on the sample surfaces

Based on their topographical properties and the bacterial response, three latex surfaces (including bare glass as control) were chosen for studying the surfaceome (all matrix-associated proteins) of 24-h biofilms formed on such materials. Surface proteins were recovered by trypsin shaving and the protein concentration was estimated. As expected, a high protein concentration was clearly apparent under the WP assay, although there was no statistically significant difference in total protein concentration among the surfaces when compared within the same biofilm-forming assay (Fig. S6).

The first examination of the proteomic data set was based on the number of MS/MS protein identifications for both biofilm formation assay (Fig. 3). When biofilms were grown using the WP assay, approximately 50% more proteins were identified compared to the AP-based assay (1317 and 935 protein identifications, respectively). Altogether, 382 proteins were uniquely detected in biofilms grown under the WP condition. It is also of interest to mention that a large majority of the protein identifications were shared by both experimental assays, particularly in biofilms formed on the 30% PS and 60% PS surfaces (Fig. 3).

The dataset of protein surfaces was grouped by the surface type (30%, 50%, 60% PS, and glass), and evaluated by their physicochemical distributions in terms of hydropathicity (Fig. S7) and isoelectric point (Fig. S8). The distribution of the GRAVY indices was similar across all the samples, with a maximum peak detected at –0.4 in each surface materials (Fig. S7). In Fig. S8, it is shown that there is no difference in neither predicted isoelectric point *(pI)* values nor weight diversity among the surfaceomes identified from biofilms on the tested surfaces (paired comparison of surfaces between methods). Furthermore, since the *pI* value is related to the subcellular localisation, the proteins in the basic region might correspond to the integral membrane/transmembrane domain proteins (TMP). Here, the used shaving protocol enabled identifying 23.3% (172 proteins) of all the predicted TMPs (Fig. S9).

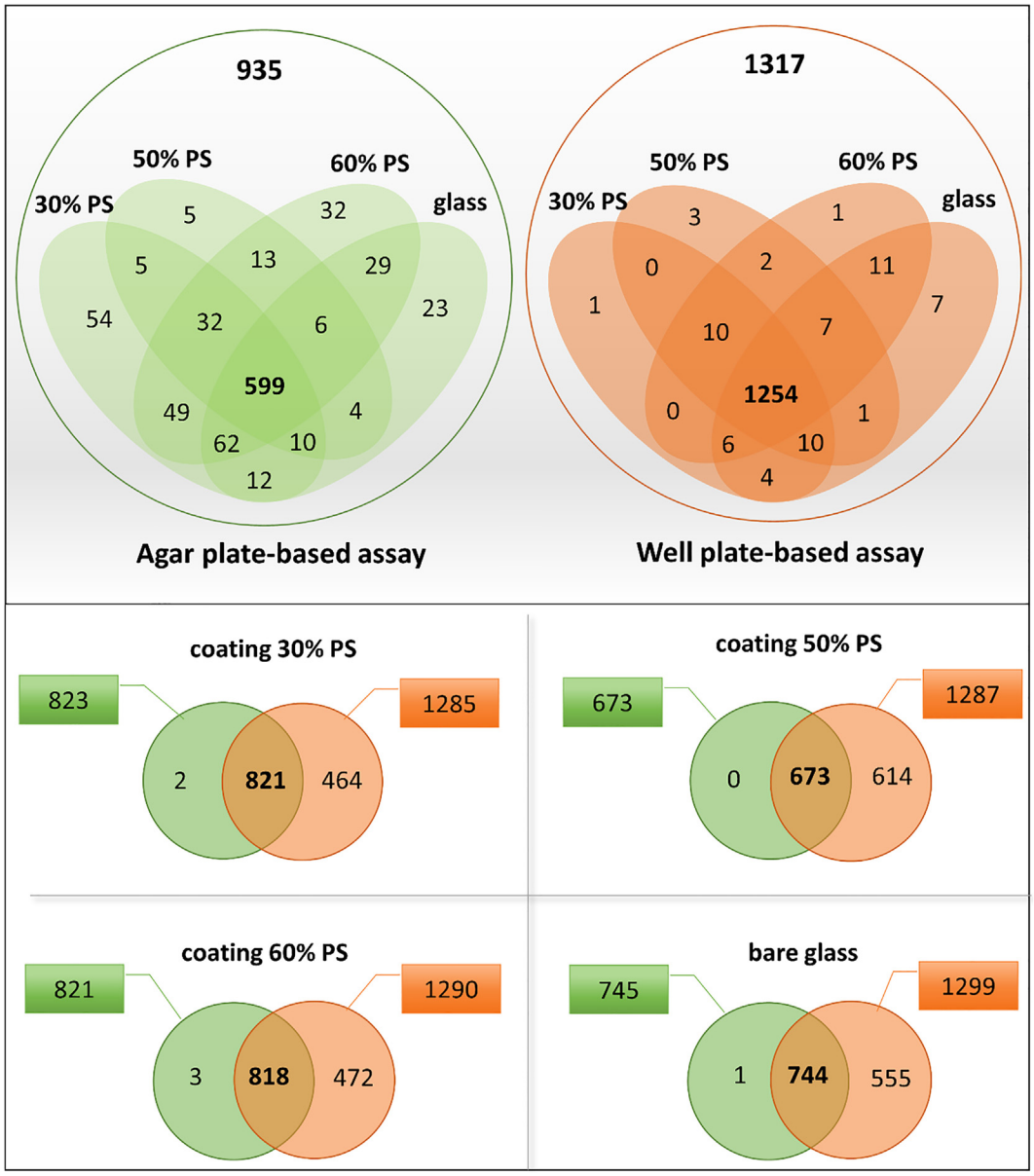

Fig. 3. Venn diagrams showing the number of protein identifications by surface type in two biofilm-forming assays. Valid identifications were considered when the proteins were presented in at least two out of three of the replicate samples of each surface.

Altogether, the broad distribution range of *pI* values, the elevated yield of identified TMP and the presence of considerable amount of highly hydrophobic proteins suggest that the applied surface shaving method benefited the extraction of a variety of functional proteins, which makes it particularly advantageous and validates the quality of the obtained proteome for studying the surfaceome.

3.2.6. Protein abundances impacted by the properties of the material surfaces

The proteome data were further subjected to multivariate analysis. Hierarchical clustering was performed on Z-score normalised, log_2-transformed LFQ intensities. Two clusters emerged based on the experimental assay used, with the largest number of up-regulated proteins belonging to the biofilms grown under the WP-based assay (Fig. S10a). Furthermore, a principal component analysis (PCA) indicated that the component 1 (explaining 61.8% of total variance) clearly grouped the proteins according to the experimental condition used (Fig. S10b). As expected, the Gene Ontology (GO) term and pathway analyses (KEGG) on the identified surfaceomes indicated that the most significantly enriched functional and metabolic pathways were the biofilms grown in the WP-based biofilm assay (Fig. S10c-d). Two accessory factors involved in the protein translation (tRNA) were the most significantly enriched GO terms, followed by GO terms associated with organic acids (carboxylic, monocarboxylic) metabolic process. The four presented KEGG pathways showed similar rank-based enrichment for aminoacyl-tRNA biosynthesis, glycolysis, tyrosine metabolism and biosynthesis of amino acids.

According to ANOVA (permutation-based FDR 0.1), 49 proteins were found to statistically differ in abundances among the studied surfaces in biofilms formed in the AP assay, while 106 proteins were statistically differing in the WP assay (the proteins are listed in Table S2 and S3). Since these proteins belong to a variety of functional groups, only known clinically relevant protein functions were systematically explored and discussed in this study. These include cell wall-anchored proteins (CWP) and proteins secreted to the extracellular milieu, which are of interest due to their role in the pathogenesis of *S. aureus* infection, as well as pathogenic moonlighting proteins and proteins that participate in the evasion of the host immune response. Based upon this, biofilms formed in the AP assay expressed 11 proteins with pathogenic functions plus two groups of moonlighting proteins (glycolytic proteins [4 proteins] and ribosomal proteins [10]) (Table 3). In biofilms formed in the WP assay, 10 proteins were identified with pathogenic function, plus four groups of moonlighting proteins (lipid enzyme [1 protein], amino acid enzymes [3 proteins], glycolytic proteins [4 proteins], and ribosomal proteins [13 proteins]) (Table 4). The network visualisation of these proteins was performed using the STRING database [47] (Fig. S11a-b), where the elevated number of edges between the identified bacterial virulence proteins suggested high degree of connectivity among the proteins that were differentially expressed in the studied surfaces. Therefore, most proteins (25 out of 49) on the surfaceome of the biofilms formed on the AP assay appeared to have virulence-related functions (Table 3), while 31 proteins out of 106 were associated to virulence in WP condition (Table 4). Taken together, using the AP assay for growing biofilms seemed to allow higher detection of *S. aureus* virulence-associated proteins among all the studied surfaces.

3.2.7. Proteomic data correlated with surface roughness

To investigate if the experimental assay and/or material surface affect the protein export or abundance of 24-h *S. aureus* biofilms, we examined more closely a set of proteins with reported virulence/pathogenic features and associated the results with surface roughness parameters. A special focus was put on those parameters that proved influential when correlating *S. aureus* viability and relative PNAG content with roughness parameters (Figs. S12–S29).

During the analysis, the abundance of several individual proteins was discovered to correlate with some of the roughness parameters found to cause a response in *S. aureus* viability and PNAG content. The observed correlations were typically rather linear (33 of 40 for the AP assay and 59 of 63 for the WP assay; see Table S4), as more complex correlations could not be reasonably interpreted from such few data points. To the best of our knowledge, no previous detailed reports of protein expression correlated with surface properties, specifically roughness parameters, have been published.

An overview of the observed responses to roughness parameters is given in Tables 3 and 4 (See Tables S4–S6 for details). For biofilms grown on the AP-based assay, correlations were observed for all but six of the chosen proteins (Tables S4 and S5). The rest of the proteins formed two groups. The first group are proteins that responded to the S_q, S_{cl37}, S_q/S_{cl37}, S_{dr}, and S_{vk} and not following similar trends as the viability (CFU). Both protein EsaA and biocomponent gamma-hemolysin HlgAB subunit A fitted in the first group. The second group was those that had a similar trend or inverse trend as the viability and responded to the "fine-texture parameters", S_{fd}, S_{ds}, and S_k as well as S_{pk}/S_k (Fig. 4a). Lipoteichoic acid synthase stands out as the response to the parameters was opposite to that of the others of this second group. Catalase and IMP dehydrogenase are also worth noting, as the glass surface data points fit the same trend as the latex data.

For biofilms grown on the WP-based assay, more pronounced responses to the surface properties were obtained in the proteomics data than in the viability and the PNAG-associated signal (Figs. S12–S29). For the selected set of 31 proteins, only three showed no apparent correlation with the roughness parameters (Tables S4 and S6). Two driving topographical properties were the parameters S_q and S_{cl37}. Those protein detections that showed a proportional correlation to the S_q typically showed an inverse correlation with the S_{cl37}. In fact, this holds true for all parameters and all proteins (if non-correlations are ignored) except for the glyceraldehyde-3-phosphate dehydrogenase 1 whose correlation with Scl_{37} did not follow this pattern. It is important to mention that the complement convertase inhibitor Efb and fibrinogen binding protein, which showed no response to the surface properties in the AP assay, did display correlation with most parameters under WP condition. Parameters of note are S_{pk}/S_k, which correlated with 7/10 investigated protein detections, and S_{cl37}, that correlated with the abundance of 6/10 proteins, as well as S_k and S_{pk}, that both correlated with 6/10 proteins (Fig. 4b).

The correlations, which are summarised in Table S4, mostly showed a very good correlation strength when analysed for Pearson's *r* and Student's *t*-test – typically at $r \geq 0.8$ and $t \leq 1.68 \times 10^{-2}$ (see details in Tables S5 and S6, respectively).

4. Discussion

The process of bacterial adhesion is complex and specific for every bacterial species. Several factors are implicated in the bacteria colonisation including the immediate environment around the substrate and the conditions for cell growth (i.e. nutrient source, growth factors, shear environment, humidity, and temperature) [50]. In this manner, the selection of the biofilm formation assay as well as the biofilm quantification method should be carefully evaluated, as minimal variations in the experimental setup can alter the bacterial biofilm growth, biofilm architecture, composition, and as consequence the outcomes of the study [51,52]. Static models are described as batch cultures given that the cells grow in

Table 3
Virulence-associated proteins identified in 24-h *S. aureus* biofilms using the AP-based assay. The proteins were classified by their Gene Ontology (GO) annotations [48], and only a single GO function is displayed when several functions were described. The secretory pathway was predicted by using Signal 5.0 engine [49]. SP, signal peptide (Sec/SPI); NC, non-classical; NP, none predicted. Roughness parameters, or the viability (CFU), with which the protein detection appeared to correlate strongly (Pearson's $r \geq |0.8|$) with are given in the rightmost column.

	Entry name	*Staphylococcus aureus* - Protein function	Gene	GO biological process	GO cellular component	Secretion	Correlating parameters
Pathogenic function	WP_000728940	Protein EsaA	*esaA*	pathogenesis	integral component of membrane	SP	S_q, S_{cl37}, S_q/S_{cl37}, S_{dr}, S_{vk}, S_{pk}/S_{vk}
	WP_077670283	MSCRAMM family adhesin SdrE	*sdrE*		cell wall	SP	—
	WP_000791575	Complement convertase inhibitor Efb	*fib*	pathogenesis	extracellular space	SP	—
	WP_000594516	Bi-component gamma-hemolysin HlgAB subunit A	*hlgA*	pathogenesis	extracellular space	SP	S_{cl37}, S_q/S_{cl37}, S_{dr}, S_{vk}, S_{vk}/S_k
	WP_000264071	IMP dehydrogenase	*guaB*	GMP biosynthetic process		NP	CFU, S_{fd}, S_{ds}, S_k
	WP_000897132	ATP-dependent Clp protease ATP-binding subunit ClpC	*clpC*	pathogenesis		NP	—
	WP_000098285	Lipoteichoic acid synthase	*ItaS*	cell wall organisation	extracellular space	NC	CFU, S_{fd}, S_{ds}, S_k, S_{pk}/S_k
	WP_000728713	Immunoglobulin G-binding protein A	*spa*	pathogenesis	cell wall	SP	CFU, S_{fd}, S_{ds}, S_k, S_{pk}/S_k
	WP_000645754	5′-nucleotidase adenosine synthase AdsA	*adsA*		cell wall	SP	CFU, S_{fd}, S_{ds}, S_k, S_{pk}/S_k
	WP_000089857	Catalase	*katA*	hydrogen peroxide catabolic process		NC	CFU, S_{fd}, S_{ds}
	WP_000522388	Nitroreductase		cellular response to oxidative stress		NC	CFU, S_{fd}, S_{ds}, S_k, S_{pk}/S_k
Glycolytic process	WP_000068176	Pyruvate dehydrogenase E1 component subunit beta	*pdhB*	glycolytic process		NP	—
	WP_001232655	Pyruvate kinase	*pyk*			NP	S_{cl37}. S_{vk}/S_k
	WP_000260117	Dihydrolipoyl dehydrogenase	*pdhD*	cell redox homeostasis	cytoplasm	NP	S_{fd}, S_{ds}, S_k
	WP_000846637	L-lactate dehydrogenase	*ldh2*	glycolytic process	cytoplasm	NP	—
Ribosomal proteins	WP_000048060	30S ribosomal protein S21	*rpsU*	translation	ribosome	NC	S_{fd}, S_{ds}, S_k, S_{pk}
	WP_000090514	30S ribosomal protein S4	*rpsD*	translation	small ribosomal subunit	NP	CFU, S_{fd}, S_{ds}, S_k, S_{pk}, S_{pk}/S_{vk}
	WP_000766074	50S ribosomal protein L15	*rplO*	translation	large ribosomal subunit	NP	S_k
	WP_001274017	30S ribosomal protein S20	*rpsT*	translation	cytosol	NC	S_{fd}, S_{ds}
	WP_000124353	30S ribosomal protein S19	*rpsS*	ribosomal small subunit assembly	cytosolic small ribosomal subunit	NP	S_{fd}, S_{ds}
	WP_000268754	30S ribosomal protein S16	*rpsP*	translation	ribosome	NC	S_{cl37}, S_{dr}, S_{vk}, S_{vk}/S_k
	WP_001074619	50S ribosomal protein L1	*rplA*	maturation of LSU-rRNA	cytosolic large ribosomal subunit	NC	S_{cl37}, S_q/S_{cl37}, S_{vk}, S_{vk}/S_k
	WP_000133953	30S ribosomal protein S1	*rpsA*		ribosome	NP	–
	WP_000572248	16S rRNA (cytosine(967)-C(5))-methyltransferase RsmB	*sun*	regulation of transcription	cytoplasm	NP	CFU, S_{fd}, S_{ds}, S_k, S_{pk}, S_{pk}/S_k
	WP_000547687	50S ribosomal protein L24	*rplX*	translation	ribosome	NC	CFU, S_{fd}, S_{ds}, S_k, S_{pk}, S_{pk}/S_k
	WP_000916187	50S ribosomal protein L27	*rpmA*	translation	cytosolic large ribosomal subunit	NC	S_{fd}, S_{ds}, S_k

Table 4
Virulence-associated proteins identified in 24-h *S. aureus* biofilms using the WP-based assay. The proteins were classified by their Gene Ontology (GO) annotations [48], and only a single GO function is displayed when several functions were described. The secretory pathway was predicted by using Signal 5.0 engine [49]. SP, signal peptide (Sec/SPI); NC, non-classical; NP, none predicted. Roughness parameters, or the viability (CFU), with which the protein detection appeared to correlate strongly (Pearson's $r \geq |0.8|$) with are given in the rightmost column.

	Entry name	*Staphylococcus aureus* - Protein function	Gene	GO biological process	GO cellular component	Secretion	Correlating parameters
Pathogenic function	WP_000069298	Elastin-binding protein EbpS	*ebpS*		integral component of membrane	NC	S_{cl37}, S_{ds}, S_k, S_{pk}/S_k, S_{pk}/S_{vk}
	WP_000279414	Glyceraldehyde-3-phosphate dehydrogenase 1	*gapA*	NADH regeneration	cell wall	NP	CFU, S_q, S_{cl37}, S_q/S_{cl37}, S_{ds}, S_k, S_{pk}, S_{vk}, S_{pk}/S_k, S_{vk}/S_k, S_{pk}/S_{vk}
	WP_000669728	Protein MAP	*map*			SP	–
	WP_000827736	Cysteine protease staphopain A	*sspP*	pathogenesis	extracellular region	SP	CFU, S_q, S_{fd}, S_{ds}, S_k, S_{pk}, S_{pk}/S_k
	WP_001574556	Thermonuclease	*nuc*	pathogenesis	integral component of membrane	SP	S_q, S_{cl37}, S_q/S_{cl37}, S_{dr}, S_{pk}, S_{vk}, S_{pk}/S_k, S_{pk}/S_{vk}
	WP_000791575	Complement convertase inhibitor Efb	*fib*	pathogenesis	extracellular space	SP	CFU, S_q, S_{cl37}, S_q/S_{cl37}, S_{dr}, S_{fd}, S_{ds}, S_k, S_{pk}, S_{pk}/S_k
	WP_076050774	Teichoic acid ribitol-phosphate polymerase TarK	*tarK*	cell wall organisation	plasma membrane	NP	S_q, S_{cl37}, S_q/S_{cl37}, S_{dr}, S_{pk}, S_{vk}/S_k, S_{pk}/S_{vk}
	WP_000919764	Penicillin-binding protein 2	*ftsI_1*	cell division	integral component of membrane	NC	CFU, S_{dr}, S_{fd}, S_{ds}, S_k, S_{pk}, S_{pk}/S_k
	WP_000034716	Molecular chaperone DnaK	*dnak*	cellular response to heat	cytoplasm	NC	–
	WP_000739205	Fibrinogen-binding protein	*fib_1*		extracellular space	SP	CFU, S_q, S_{cl37}, S_q/S_{cl37}, S_k, S_{vk}, S_{vk}/S_k, S_{pk}/S_{vk}
Lipid metabolism	WP_000047355	Malonyl CoA-ACP transacylase	*fabD*	fatty acid biosynthetic process		NP	S_q, S_{cl37}, S_{pk}, S_{pk}/S_k, S_{pk}/S_{vk}
Carbohydrate degradation	WP_000717560	ATP-dependent 6-phosphofructokinase	*pfkA*	fructose 6-phosphate metabolic process	cytoplasm	NP	S_q, S_{cl37}, S_q/S_{cl37}, S_{dr}, S_{pk}
	WP_000161314	Glucokinase	*glkA*	glycolytic process	cytoplasm	NP	S_q, S_{cl37}, S_q/S_{cl37}, S_{dr}, S_{pk}
	WP_001232655	Pyruvate kinase	*pyk*	NADH regeneration		NP	S_{cl37}, S_{fd}, S_{ds}, S_k
	WP_001127959	Mannose-6-phosphate isomerase	*gmuF*	carbohydrate metabolic process		NP	CFU, S_{fd}, S_{ds}, S_k, S_{pk}, S_{pk}/S_k
Amino acid catabolism	WP_000411087	D-alanine aminotransferase	*dat*	D-amino acid biosynthetic process		NP	CFU, S_{cl37}, S_{fd}, S_{ds}, S_{pk}, S_{pk}/S_k
	WP_000210828	Serine/threonine dehydratase	*tdcB*	L-serine catabolic process		NP	S_q, S_{cl37}, S_q/S_{cl37}, S_{dr}, S_{pk}, S_{vk}, S_{pk}/S_k, S_{vk}/S_k, S_{pk}/S_{vk}
	WP_000289134	GTP pyrophosphokinase	*ywaC*	guanosine tetraphosphate metabolic process		NP	S_q, S_{cl37}, S_q/S_{cl37}, S_{dr}, S_{pk}, S_{vk}, S_{vk}/S_k, S_{pk}/S_{vk}
Ribosomal proteins	WP_000916187	50S ribosomal protein L27	*rpmA*	translation	cytosolic large ribosomal subunit	NC	S_{cl37}, S_q/S_{cl37}, S_{dr}, S_{vk}, S_{vk}/S_k
	WP_000090796	30S ribosomal protein S13	*rpsM*	translation	cytosol	NP	S_q, S_{cl37}, S_q/S_{cl37}, S_{vk}, S_{pk}/S_{vk}
	WP_000048060	30S ribosomal protein S21	*rpsU*	translation	ribosome	NC	S_{cl37}, S_q/S_{cl37}, S_{dr}, S_{vk}, S_{vk}/S_k
	WP_001790547	30S ribosomal protein S9	*rpsI*	translation	ribosome	NP	S_{cl37}, S_q/S_{cl37}, S_{dr}, S_{vk}
	WP_000766074	50S ribosomal protein L15	*rplO*	translation	cytosolic large ribosomal subunit	NP	S_q, S_{cl37}, S_q/S_{cl37}, S_{pk}, S_{vk}, S_{pk}/S_{vk}
	WP_000268484	30S ribosomal protein S2	*rpsB*	translation	cytosolic small ribosomal subunit	NP	S_q, S_{cl37}, S_q/S_{cl37}, S_k, S_{pk}, S_{pk}/S_k, S_{pk}/S_{vk}
	WP_001274017	30S ribosomal protein S20	*rpsT*	translation	cytosol	NC	S_{cl37}, S_q/S_{cl37}, S_{dr}, S_{vk}, S_{vk}/S_k
	WP_000124353	30S ribosomal protein S19	*rpsS*	cytosolic ribosomal small subunit assembly	small ribosomal subunit	NP	CFU, S_{fd}, S_{ds}, S_k, S_{pk}, S_{pk}/S_k, S_{pk}/S_{vk}
	WP_000529877	30S ribosomal protein S3	*rpsC*	translation	small ribosomal subunit	NP	CFU, S_{cl37}, S_{fd}, S_{ds}, S_k, S_{pk}, S_{pk}/S_k, S_{pk}/S_{vk}
	WP_000091975	50S ribosomal protein L6	*rplF*	translation	ribosome	NC	—
	WP_001137495	30S ribosomal protein S7	*rpsG*	cytosolic ribosomal small subunit	small ribosomal subunit	NP	S_{cl37}, S_q/S_{cl37}
	WP_001074619	50S ribosomal protein L1	*rplA*	maturation of LSU-rRNA	large ribosomal subunit	NC	CFU, S_q, S_{cl37}, S_{fd}, S_{ds}, S_k, S_{pk}, S_{vk}, S_{pk}/S_k, S_{pk}/S_{vk}

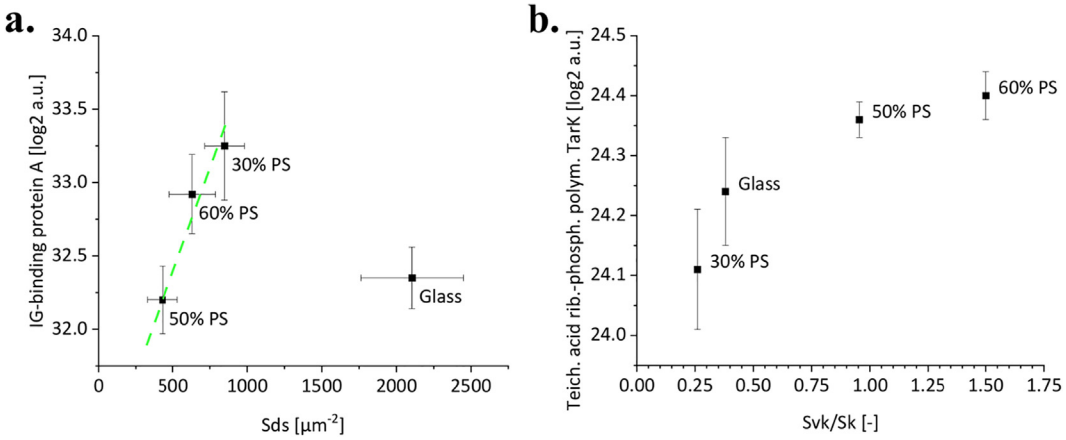

Fig. 4. Examples of correlation between protein abundances and physical parameters. In (a), detection of the Immunoglobulin G-binding protein A after AP assay on different surfaces correlated to S_{ds} (R^2(adj) = 0,8954, Pearson's *r*= 0.973, Student's *t*-test = 0.0376). The data point for glass deviates from the trend observed for the latex surfaces. In (b), the teichoic acid ribitol-phosphate polymerase TarK expression during WP assay correlated with S_{vk}/S_k. The observed correlation is interpreted being non-linear, even though it has a moderately good correlation to a linear model (R^2(adj) = 0.61254, Pearson's *r*= 0.566, Student's *t*-test = 0.0000576). Error bars indicate the 95% CI of the mean.

a fixed volume of nutrients either on solid medium or in liquid medium without any shear flow [53]. Advantages of this system involve the simplicity of the protocols, flexibility of conditions, and the fact that no specialised or expensive laboratory equipment are typically needed [54]. Furthermore, these models have shown to be practical for studying biofilm formation, on various materials, where low shear flow does not play a role (e.g., chronic wounds, ear infections) [40,42,55].

In our study, the formation of biofilms on latex-coated surfaces was studied under two static biofilm formation assays using orthogonal approaches, aiming to identify the drivers that influence the *S. aureus* colonisation. Since *in vitro* static models are commonly used for assessing the efficacy of biomaterials, an in-depth understanding of whether the experimental mode influences the outcomes in bacterial growth is highly relevant. The main difference between the used biofilm-formation assays is the state of the nutrient source. While in the AP-based assay the TSA-agar was the base of nutrients that diffused to the materials through a filter membrane [42,56], in the WP-based assay the TSB was the nutrient medium that was added simultaneously with the bacteria suspension to the 12-WP. In consequence, the biofilm formation in these assays takes place on a filter-surface interface and on a solid–liquid interface, respectively. The surface-area-to-volume ratio was another factor that differed in these assays as it was over 15 times higher in the AP assay (Table 2).

Despite demonstrating a generally lower count of viable *S. aureus*, the AP-based assay allowed the detection of significant differences in the level of biofilm colonisation on the set of surfaces which led to consistent outcomes (i.e., small variances among the repetitions) (Fig. 2a). In turn, the usage of the WP-based assay resulted in a higher amount of attached viable cells, PNAG content, and number of identified proteins, when compared to results of similar latex surfaces from the AP assay (Fig. 2a-c). Since distinctive trends of the *S. aureus* colonisation were determined among the studied surfaces based on the biofilm-forming conditions, it suggests that the surrounding microenvironment, as well as the particular physicochemical and topographical features of the tested surfaces, directly affects the bacteria colonisation mode.

4.1. Physico-chemical properties of the surfaces vs. viability of S. aureus

The least hydrophilic surfaces, 80% and 100% PS, caused a slightly lower viability of *S. aureus* biofilms in the AP assay (Table 1 and Fig. 2a). These surfaces had the highest water contact angles (about 80° and 91°) and the lowest polar negative surface energy components of the latex surfaces used (6 mJ/cm^2 and 0.5 mJ/cm^2) (Figs. S12 and S13). Furthermore, the viability apparently decreased with increasing total or dispersive surface energy (Figs. 1 and S14). The three surfaces with the highest number of *S. aureus* biofilm cells (40%, 50%, and 60% PS) also were the roughest samples regarding the parameters S_{dr} and S_q (see Table S1). In this regard, 0% PS and 20% PS, which were the flattest surfaces among the tested materials, appeared as outliers with a higher observed viability than the suggested trend. Of note, these two surfaces often appeared as outliers in correlation plots of bacterial viability against roughness parameters in the AP-based assay thus indicating that other surface properties might also influence the viability. In the measurements in the WP-based assay, the least hydrophilic 100% PS surface showed one of the lowest viabilities, but small statistical differences make such interpretations mostly speculative. Regarding surface chemistry, the 70% PS surface, which yielded the highest viability in the WP-based assay, had an average water contact angle and dispersive surface energy. No clear trend was observed between the chemical parameters and viability in this biofilm growth assay.

Interestingly, the biofilm viability on the latex surfaces did not appear to clearly correlate with the commonly used roughness parameters (S_{dr} and S_q) in the studied roughness interval (see Fig. 5a, and Figs. S15 and S18) in any of the biofilm-forming assays used here. A general trend that a rougher surface increases the bacterial viability [57], was not obvious in our observations (Fig. 5a). Alternatively, the normalised roughness S_q/S_{cl37} appeared to correlate slightly better with the increase in bacterial viability for the AP assay (Fig. S17). Adhesion maxima have previously been observed by e.g. Chatterjee et al. [58], but our data provides only a weak indication of a maximum for a S_q/S_{cl37} around 0.08–0.16. The 0% PS and 20% PS surfaces also stand out as outliers for these parameters. Conversely, no clear trend was observed for this parameter in the WP-based assay.

Good correlations with the viability of the biofilm cells on the surfaces in the AP-based assay were observed for the following parameters: First, S_{fd}, S_{ds} and S_k showed a rather linear correlation with the viability for this AP assay (Fig. 5b, and Figs. S19, S20, S23). These are discussed here together due to the interesting feature of the surfaces – these three parameters, S_{fd}, $S_{ds,}$ and S_k, were linearly correlated to each other (Fig. S28). More importantly, they all appeared to drive the viability similarly. The viability decreased

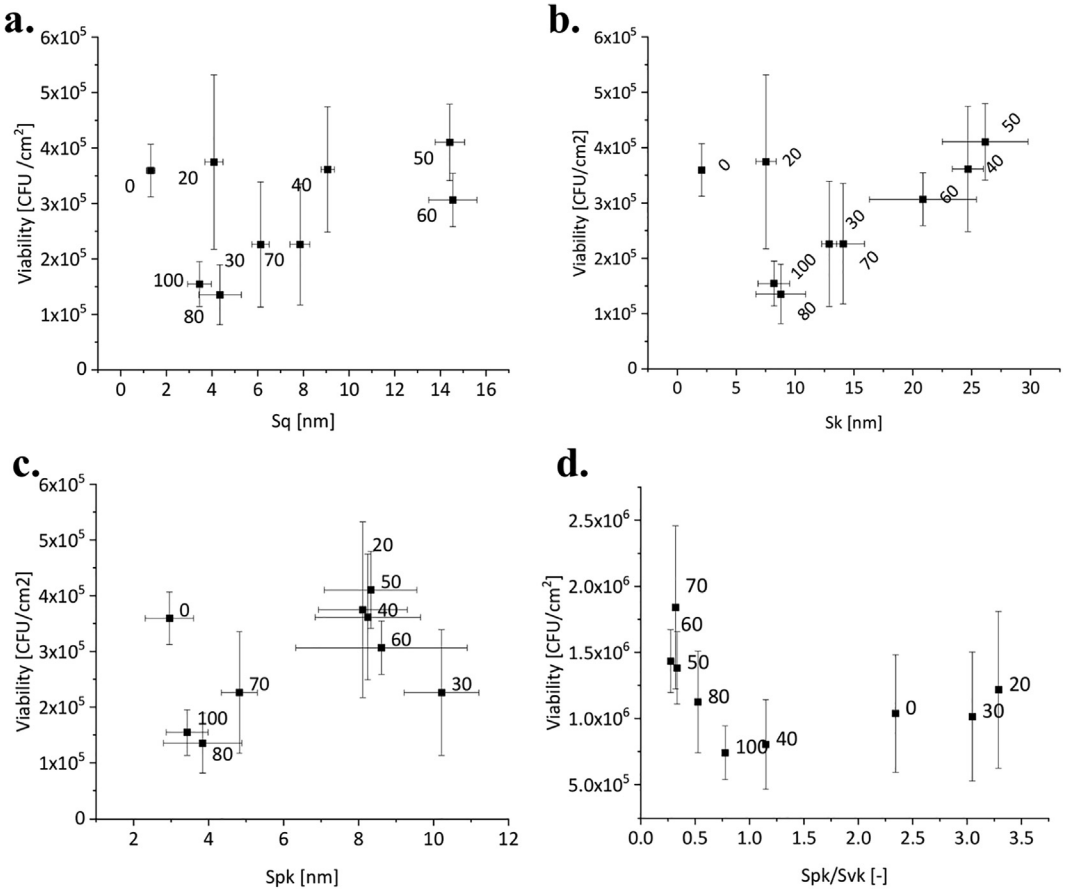

Fig. 5. *S. aureus* viability in relation to roughness parameters for biofilms grown in the AP-based assay: (a) S_q, (b) S_k, and (c) S_{pk}, and the WP-based assay (d) S_{pk}/S_{vk}. Error bars indicate the 95% CI of the mean.

when the S_{fd} increased from 2 to 2.2. 0% PS and 20% had a higher S_{fd} and a comparatively high viability. Similarly, decreasing the S_{ds} below 1500 $1/\mu m^2$ appeared to increase the viability, but three samples appeared as outliers (0%, 20%, and 70%). More readily associable with actual surface geometry is perhaps the S_k which showed a linearly increasing viability with an increasing S_k above 10 nm (Fig. S23). In this case, the 0% and 20% PS surfaces had lower S_k but biofilms on them showed a rather high viability, much like the correlation plot for the S_{fd}. These parameters all point to the biofilm growth-driving effect of the core texture features of the surface. An interesting trend was also seen for the S_{pk} (Fig. S22). A maximum was observed at a S_{pk} of about 7–8 nm. The smoothest surface in this data set, the 0% PS, was an outlier (Fig. 5c). Altogether, these correlations could be interpreted to show an affinity of *S. aureus* for surfaces with a roughness increased by fine nanoscale structures rather than surfaces with a large-scale coarseness. This interpretation holds true even when considering the S_{pk}, which expresses peak formations with the highest peaks removed, i.e., the low-height topographies.

Additionally, in the AP-based assay, plotting the *S. aureus* viability against S_{pk}/S_k gave a good correlation between roughness and viability (Fig. S24). The plot showed a linearly increasing viability on both sides of the minimum, that was found at 0.45–0.5 ratio of S_{pk}/S_k. An increasing S_{pk}/S_k appeared to have a lesser effect on viability than the decrease below said minimum. A similar but somewhat more ambiguous trend was observed for S_{vk} (Fig. S25), where the lowest viability was found at a S_{vk} of approx. 7.5 nm, and the viability increased for higher and lower values of this roughness parameter. This data indicates that while a rougher surface was preferred in these conditions, the relative dominance of peak or valley features in the surface texture are also important for the colonisation of bacteria in this growth assay.

With respect to the biofilms formed in the WP-based assay, the correlations with surface roughness were less obvious probably due to the small statistical differences between microbial data of each surface. In general, an increasing roughness slightly increased the viability when considering the classic parameters S_q, $S_{dr,}$ and S_q/S_{cl37} (see Figs. S15, S17, S18). Plots of the viability against the S_{cl37} on the other hand showed a trend, with a maximum viability at average values of the parameter (approx. 90 nm) (Fig. S16). Here, the parameters S_{fd} and S_{ds} did not show a correlation with the viability (Fig. S19 and Fig. S20). As shown in the AP assay, the S_{pk}/S_k parameter showed a correlation with the viability, even if S_{pk} or S_k alone did not do so. The surfaces with a larger S_{pk}/S_k appeared to have a lower viability (Fig. S24). This means that large peak structures on the surface were unpreferred for *S. aureus*. Noteworthy was also the correlation with S_{vk}, indicating than an increased S_{vk} was more preferable, contrary to the observation in results from the AP-based assay (Fig. S25). Similarly, the S_{pk}/S_{vk} suggests that a less dominating peak structure is much preferred for *S. aureus* growth (Fig. 5d). Taken together, these three-dimensional functional parameters (S_{pk}, S_{vk}, S_k, and their combinations) emerged to best correlate with the biofilm viability in this assay. Chatterjee, et al. have also reported a periodicity, i.e., maxima and minima, in *S. aureus* and *P. aeruginosa* growth on surfaces with varying RMS-roughness [58].

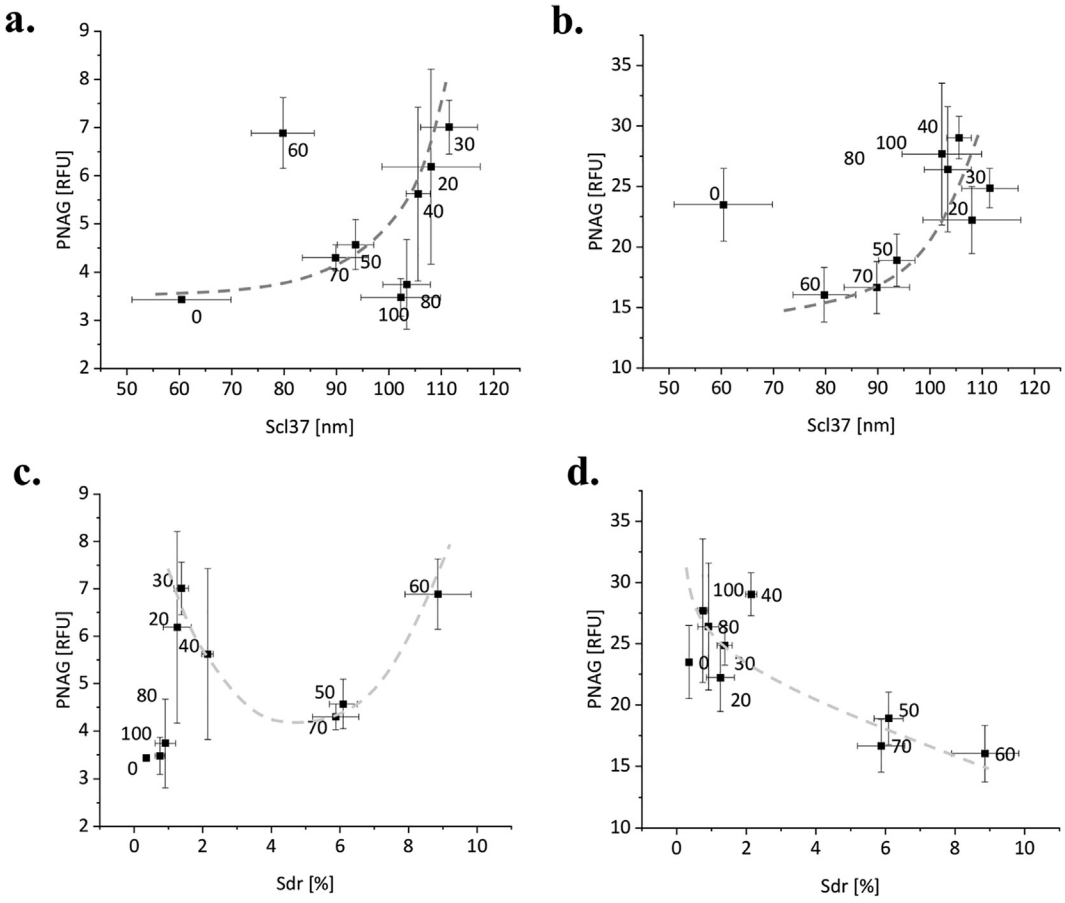

Fig. 6. The response of PNAG content in relation to roughness parameters (S_{cl37} and S_{dr}) for biofilms grown in the AP- (a, c) and the WP- (b, d) based assay. Error bars indicate the 95% CI of the mean. Dotted lines indicate the authors' interpretation of a trend.

4.2. Physico-chemical properties of the surfaces vs. PNAG-fraction abundances of S. aureus

An increasing hydrophilicity (decreasing water CA) appeared to increase the relative PNAG content in the AP-based assay on all surfaces except the 0% PS (see Table 1 and Fig. 2b-c). The lowest detection was on the 0%, 80%, and 100% PS. While 80% and 100% PS also showed a low viability, the 0% PS showed a comparatively high viability. Comparing PNAG content and biofilm viability on the different surfaces only partly explains the variations in PNAG content (Fig. S5). In the WP-based assay, the hydrophilicity of the surfaces appeared to bear no effect on the content. Indeed, in a PNAG detection vs. water contact angle plot, the PNAG detection rate appeared rather similar for all contact angles with the three roughest samples in terms of S_q and S_{dr} (Fig. S15 and Fig. S18). Similar was the case of dispersive surface energy, which showed no clear correlation. In the AP-based assay, two samples, 80% and 100% PS, often stood out as outliers when plotting correlations between the PNAG content and different topological character of the samples. This indicates an effect of their surface chemical properties on the PNAG content, and of these properties, the reduced polarity was observed to be particularly impactful. It could also be noted that for biofilms grown in the WP, these two surfaces (80% and 100% PS) had among the highest PNAG content, compared to the AP assay where these surfaces had the lowest. Overall, different surface properties again appeared to drive a different bacteria response in different growth assays.

Of the basic roughness parameters, S_q did not correlate with the PNAG content (Fig. S15). The S_{cl37}, on the other hand, did so for both growth assays (Fig. 6a–b). For biofilms grown by either biofilm growth assay, an increasing S_{cl37} increased the PNAG content. In the AP assay, 60% PS surface caused a higher PNAG content at comparatively low, approx. 77 nm, S_{cl37}. Instead, 80% and 100% PS surfaces caused a lower PNAG content, which could be attributed to the lower polarity of these surfaces. In the WP assay, the 0% PS surface with lowest S_{cl37} stood out with a higher content of PNAG than on some other surfaces. Of note is that, when comparing the PNAG abundance to the number of colonies detected, the increased PNAG abundance correlated with increasing S_{cl37}. For either biofilm growth assay, S_q/S_{cl37} did not correlate with the PNAG abundances (Fig. S17).

The S_{dr}, appeared to affect the content of PNAG in both growth assays (Fig. 6c–d). While in the WP condition an increasing S_{dr} decreased the relative PNAG (reaching a minimum at S_{dr} of 6%), it was less conclusive in the AP condition. The two least polar surfaces (80% and 100% PS) appeared as minima in the AP assay, which could be explained by the effect of surface polarity on the PNAG content. Importantly, here the groupings are the low polar surfaces and the surfaces with lowest S_{vk}/S_k (20%, 30%, and 40% PS) (Fig. S26). Furthermore, in the AP assay, the S_{fd}, $S_{ds,}$ and S_k again seemed to have an inter-comparable effect on the PNAG abundance, similarly to what was seen for the viability (Figs. S19–20 and S23). Thus, in all three cases a correlation plot with the respective parameter yielded a maximum PNAG abundance at intermediate values of the parameters S_{fd} approx. of 2.15 (span 2.05–2.35), S_{ds} approx. 750 $1/\mu m^2$ (span 400–3000 $1/\mu m^2$), and S_k of approx. 16 nm (span 2–26 nm). Two of these three points were always the two low polarity surfaces. The last of the three is either the 70% PS, in S_{fd} and S_k correlation graphs, and, in the case of S_{ds}, the 0% PS. Four surfaces (0%, 70%, 80%, and 100% PS) were those

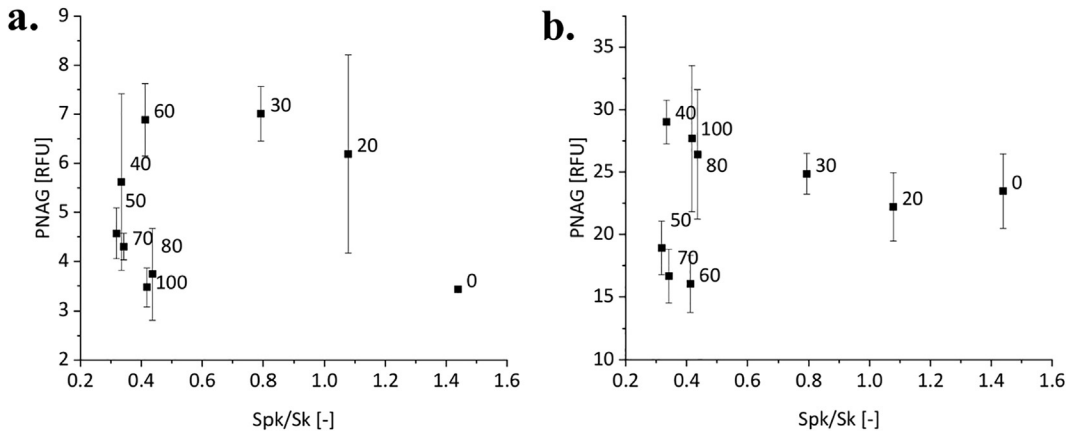

Fig. 7. The PNAG content trend with variations of S_{pk}/S_k in (a) the AP- and (b) WP-based assay. Error bars indicate the 95% CI of the mean.

with lowest S_p and S_{pk} (Figs. S21 and S22). In the WP assay, the parameter S_{ds} appeared to affect the PNAG abundance, similarly to the behaviour observed in the AP assay, with a maximum at around 1250 $1/\mu m^2$ and quickly decreasing when S_{ds} decreased (Fig. S20). Still, two of the roughest surfaces, 50% and 60% PS, appeared as outliers. Of note is also that the PNAG abundance relative to CFU seemed to decrease as the S_{ds} increased, whereas an increasing S_k appeared to decrease the PNAG content in all cases except for the 40% PS (Fig. S23).

The parameter S_{pk}/S_k had a similar effect as S_{ds} on the PNAG abundance in both assays (Fig. 7a-b; Fig. S20). In the WP condition, a slight decrease in PNAG content was seen on surfaces with more dominating peaks (i.e., increasing S_{pk}/S_k). The three samples with the highest S_q and S_{dr} (50–70% PS) appeared as outliers. In the AP condition, the expression peaked at an S_{pk}/S_k of 0.6, with a slightly lower PNAG content than the overall trend on the low polarity surfaces (80% and 100% PS). Here, the detected PNAG per the number of colonies appears to be highest at an S_{pk}/S_k of 0.8, decreasing rather linearly as the parameter increases or decreases.

An opposite trend was found for the S_{vk}/S_k, even though this parameter did not seem to correlate with the bacterial viability (see Fig. S26). In the AP assay, the PNAG abundances on the surfaces showed a clear minimum at a S_{vk}/S_k of 0.6, where either side the PNAG increased rather linearly, albeit more quickly as the S_{vk}/S_k decreased. Here, no clear trend was seen but generally the PNAG decreased as S_{vk}/S_k increased. Comparing the effect of S_{pk}/S_{vk} showed opposite responses in the assays (Fig. S27). For cultivations with the AP assay, either dominating valleys or peaks, i.e., high or low S_{pk}/S_{vk}, increased the PNAG abundance. This increase in expression appeared quicker below 1, indicating a stronger response to valley geometries. For the biofilms grown in the WP assay, the maximum PNAG amount was observed when $S_{pk}/S_{vk} \approx 1$. Increasing the relative peak height caused a slower decrease in PNAG compared to the steeper decrease with increasing relative valley depths, again indicating a stronger effect on valley geometries. As the *S. aureus* colonisation showed the opposite response to the same values and parameters of the studied surfaces, the biofilm viability could also be described to express less PNAG per CFU on surfaces with more dominating peaks or valleys. Therefore, dominating valleys appeared to decrease the relative PNAG abundance.

4.3. The combined influence of surfaces' chemical and topological properties on biofilm viability and PNAG abundance

A rudimentary attempt was made to account for the impact of surface chemical and topological surface properties on *S. aureus* biofilm growth in the AP- and WP-based assays. The most successful combinatory model was based on the S_{ds} parameter, which was examined due to its driving effect on *S. aureus* viability in both assays (see Fig. S20). Particularly intriguing was its linear appearance with the two rough surfaces (50% and 60% PS) appearing above the main grouping of data points, and two data points for the smoothest surfaces (0% and 100% PS) lying slightly below the main grouping. Combining this hybrid "fine-structure" parameter S_{ds} with a height parameter, specifically S_q or S_{10z}, formed the viability data into a somewhat more linear trend (Fig. S29). Thus, for both biofilm assays, the data points were observed to be grouped in accordance with the surface chemical parameters, as was discussed in Section 4.1. In the case of bacterial viability data of the WP assay, accounting for a surface chemical parameter, the water CA or dispersive surface chemistry, which both were deemed possible influencers of the viability, yielded an interesting trend. The best indicative fit (with an R^2 adjusted of 0.80 and a Pearson's r of 0.91) was found for the following combination of parameters:

$$\left(S_{ds} \cdot S_q\right)^{\frac{1}{CA}}.$$

The resulting curve is presented in Fig. 8. Strikingly, also the PNAG abundance data plotted against the same parameter yielded a reasonably good fit (R^2 adjusted of 0.60 and a Pearson's r of −0.81). A surface with more adsorption sites of higher height that also is more hydrophilic or has a lower dispersive energy (according to an almost as good linear trend for the combined parameter $\left(S_{ds} \cdot S_q\right)^{\frac{1}{CA}}$) appeared more viable for the *S. aureus* biofilm in the WP assay. On such surfaces the bacteria also produced less PNAG, possibly indicating less stress when attaching to the underlying surface.

Attempting to describe the response in the AP assay data with the same parameters did not give a clear trend for the viability data. However, a fair trend for PNAG was observed, where PNAG increased with an increasing combined parameter (Fig. 8), thus diverging from what was observed for the WP assay. A better model (with an R^2 adjusted of 0.81 and a Pearson's r of 0.90) related to the biofilm viability in the AP assay was obtained when emphasising the height parameter (S_{10z}) and accounting for the polar negative surface energy component (Pol-), rather than other surface chemical parameters. The influence of this parameter rather than wetting or dispersive surface energy was suggested by the plots of surface chemical parameters versus viability and the grouping after the initial combination of roughness parameters. The best model obtained was:

$$\frac{1}{\left(S_{ds} \cdot S_{10z}^2\right)^{\frac{1}{Pol}}}.$$

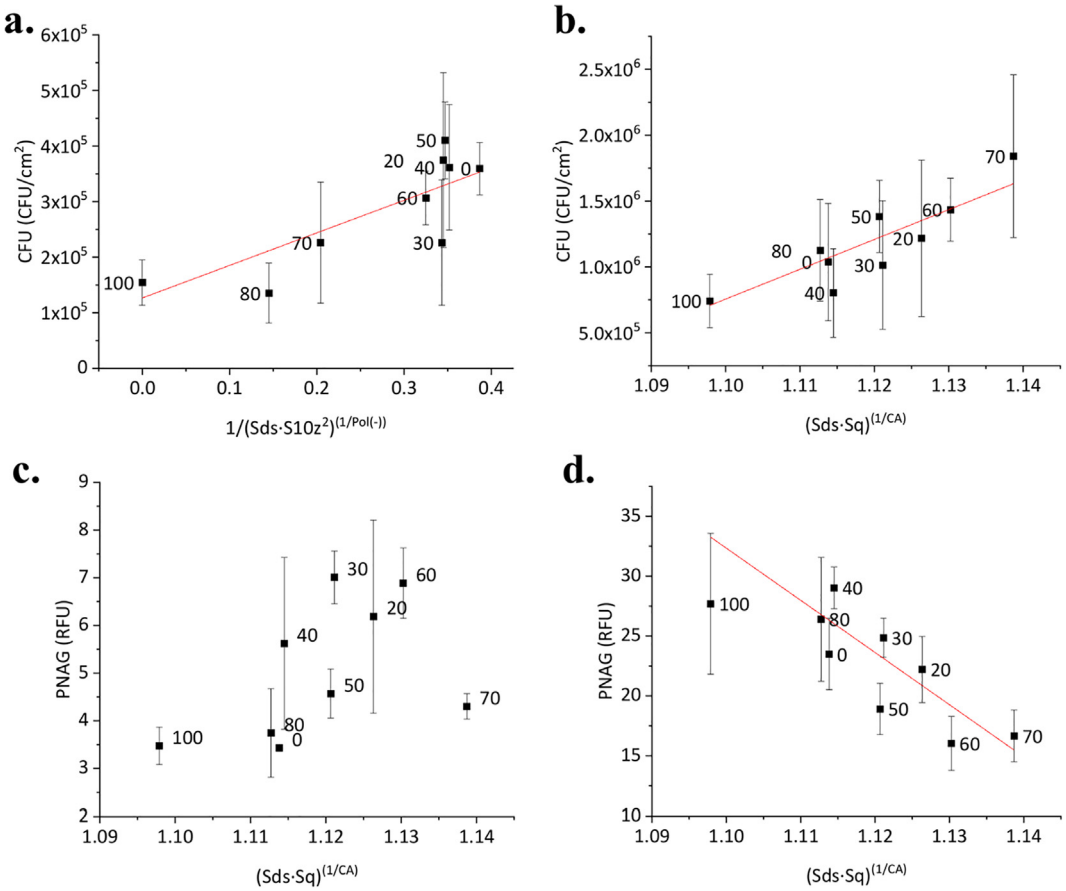

Fig. 8. The best fitting models and a linear fit for viability data from AP- and WP-based assay (a. and b.) viability data and PNAG content data from AP- and WP-based assay (c. and d.). Linear fit intentionally omitted from AP assay PNAG data plot due to 70% sample being an outlier. Error bars show a 95% CI of the mean.

This approach, however, did not seem to fit any other data well. In this case, the driving properties were the polar surface chemical properties and the height parameter, specifically the highest heights as given by the S_{10z} rather than variations of the overall surface which is more described by S_q. Yet in this case, an increasing topographical contribution decreased the biofilm viability.

While the differences in the responses of the biofilms cultivated in different milieus is highlighted by the different approaches needed to explain the two sets of viability data, a core similarity is suggested by the common parameters used – a height parameter, S_q or S_{10z}, and the S_{ds} as well as a surface chemistry component. The convergence of these parameters fits a DLVO or xDLVO model of bacterial attachment [8,9,17], but these theories are limited to describe the initial bacterial adhesion onto the surface whereas here 24-h biofilms were studied. Therefore, here we propose that summits, or attachment loci, spread over the surface (S_{ds}) allow for an easier irreversible bacterial attachment when further away (higher S_q or S_{10z}) from the bulk of the potential barrier caused by particle–surface interactions (Fig. S29).

4.4. S. aureus surfaceomes were affected by the surface properties of the materials

The impact of the biofilm growth assays was also revealed in the differences of protein abundance profile. The hierarchical clustering as well as the principal component analysis approach clearly grouped the abundances of the proteome profile in response to a change in the assay type (Fig. S10a-b). This outcome agrees with the denotation of surface proteins since they are displayed in the cell surface based on their interaction with their surrounding environment [59]. When comparing the *S. aureus* surfaceome enrichment between both biofilm-forming assays, the GO terms as well as the KEGG pathways indicated that the WP assay showed significantly enriched protein functions (Fig. S10c–d), which is in line with the results of other biofilm components quantified herein (viable cell density and PNAG abundance). Although the identified metabolic pathways mainly consist of proteins with known intracellular functions, their presence on the cell surface and/or in the extracellular matrix of the biofilm may indicate that they are deliberately secreted, and are thus playing multiple roles [60,61]. These so-called moonlighting proteins comprise of a subset of proteins that cause a variety of physiological and biophysical functions, and may be considered as important virulence factors [62]. The glycolytic/gluconeogenesis pathway, one out of the four metabolic pathways highly enriched, contained enzymes such as glyceraldehyde-3-phosphate dehydrogenase, phosphoglycerate kinase, lactate dehydrogenase, glucokinase, enolase, and pyruvate dehydrogenase. Importantly, many proteins of the carbohydrate metabolism pathway, such as glycolytic enzymes, have been shown to moonlight in the cell surface as mediators of host factor attachment in several species, including *S. aureus* [60,63]. The other enriched pathway was composed of several proteins that participate in the aminoacyl-tRNA biosynthesis, which have an essential role in cell viability [64]. It is important to note that these two aforementioned significantly enriched pathways, along with the tyrosine metabolism and biosynthesis of amino acid pathways, contain proteins that are induced by anaerobic growth mode [65]. Therefore, the biofilm growth assays used in this study might differ

in the level of oxygen concentration. Additionally, since oxygen availability affects the expression of virulence factors in *S. aureus* [66], it would be important to monitor such environmental signals when developing a biofilm assay.

Significant differences in abundances of the *S. aureus* surfaceome, formed on the material surfaces, were also analysed based on the growth assay type. Thus, in the AP-based assay, 49 proteins were found to statistically differ in abundances among the studied surfaces (Table 3 and Table S2). Six of these were identified as proteins with signal peptides (see Table S7), from which five of them participate in the biological process of *S. aureus* pathogenesis through different mechanisms. Within this subset of proteins, immunoglobulin G-binding protein A stood out for showing the highest abundance, particularly on the 30% PS surface where it was twice more expressed than on the glass reference and 50% PS surface. The 30% PS presented four times more protein EsaA compared to the other three surfaces, as well as of protein adhesin SdrE and fibrinogen-binding protein compared to the glass surface. In contrast, hemolysin HlgAB subunit A was about eight times more abundant on 30% PS than on the glass surface. Lipoteichoic acid synthase, a transmembrane protein that participates in the cell wall organisation and biosynthesis of lipoteichoic acid, was also identified to statistically differ in abundances among the surfaces. Considering that lipoteichoic acid is an anionic polymer surface part of the peptidoglycan wall and thus crucial for bacterial growth and cell division [67], it was intriguing that it was twice as abundant in biofilms grown on the 50% PS and glass surfaces than on the 30% and 60% PS surfaces, as the glass surface gave a low bacterial density. The group of glycolytic proteins (pyruvate dehydrogenase, pyruvate kinase, dihydrolipoyl dehydrogenase, and L-lactate dehydrogenase) identified herein, which were among the highly abundant proteins in the AP-based assay, were expressed less when grown on the 50% PS surface. Although the translocation pathways of pyruvate dehydrogenase and pyruvate kinase are unknown, these proteins have been found to moonlight as adhesins [68]. Moreover, near to one fifth of the statistically differential proteins detected on the surfaces in this growth assay belong to the group of ribosomal proteins that participate in the peptide metabolic process. Recent studies have attributed the presence of ribosomal proteins in the cell surface to their moonlighting function that contributes to biofilm integrity [69].

S. aureus biofilms grown under the WP-based assay had 106 proteins significantly differing in abundances based on the material surfaces (Table 4 and Table S3). Importantly, glyceraldehyde-3-phosphate dehydrogenase 1, a known cell surface adhesion with a role in *S. aureus* infection [68,70], was the highest abundant moonlight protein showing more expression on the glass than on the polymer surfaces. There was a marked difference in the abundance of two fibrinogen-binding proteins between the glass and 30% PS surface, where the latter was about eight times higher in abundance. Of note, fibrinogen-binding proteins are recognised as virulence factors that participate in adhesion to surfaces as well as in immune system evasion [71]. Moreover, the biofilms on the 30% PS surface also exhibited the highest abundance of cysteine protease staphopain A and MAP protein, which are classically secreted by *S. aureus* and participate in the evasion of the complement system [72,73]. In contrast, the penicillin-binding protein 2, a membrane-associated protein with transpeptidase activity that participate in cell wall biosynthesis and is the target of antibiotic activity [74], was less abundant on the same 30% PS surface. Other virulence factors, affected by the material surface, include thermonuclease Nuc (upregulated on 30% PS and downregulated on the glass surface) and chaperone DnaK (upregulated on 50% PS and downregulated on 60% PS). The former relates to the biofilm structuring and detachment, while the latter enhances invasiveness into host cells by binding to plasminogen [3,60]. Several ribosomal proteins that moonlight as mediators or stabilisers of biofilm integrity [69] were differently expressed among the surfaces. Furthermore, groups of canonically cytoplasmic proteins (lipid metabolism, carbohydrate degradation, amino acid catabolism) were also identified here. Their presence in the bacteria surface might be related to cell lyses or still uncovered mechanisms pointing to moonlight phenomena [75,76]. Previous studies have reported that *S. aureus* might deliberately secrete cytosolic proteins via membrane vesicles to improve antibiotic resistance, chronic systemic infectivity, and transference of proteins between bacteria [77].

5. Conclusions

Biofilms of *S. aureus* grown on nine different nanostructured latex surfaces with different nanotopography were investigated using two biofilm growth conditions. The bacterial response was measured as biofilm viability and PNAG abundance, as well as identification and quantification of proteins in the cell surface (surfaceome). This study demonstrates that different surface properties promote different trends for both the viability and PNAG abundances depending on the bacterial growth assay used. Thus, when *S. aureus* biofilms were formed on the nanostructured surfaces in the AP-based assay, both the viability and PNAG abundance responded to variations in surface hydrophobicity and polar negativity. Topographical properties describing the fine texture, as well as the peak and valley structures, were observed to be strongly connected to the bacterial colonisation response, whereas the lateral variations appeared to influence the PNAG content. By contrast, in the *S. aureus* biofilms formed in the WP-based assay on the same materials, both the bacterial viability and PNAG content was unaffected by the surface chemical properties. Instead, the biofilm PNAG content and viability seemed to be influenced by lateral variations and effective surface area. Parameters relating to the valley depth, fine structure, and peak height, and their relative proportions appeared to describe the features driving the *S. aureus* colonisation in terms of PNAG abundance and biofilm viability.

Our findings provide a greatly detailed description of the properties controlling the bacterial biofilm response. We also highlight the utility of using several roughness descriptors when investigating the biofilm response. Further, the difference between the *S. aureus* responses when grown in different assays underline that the choice of the biofilm-formation assay should be carefully considered, or several adequate assays should be used, particularly when investigating novel biomaterials as it might even impact the observations done on, e.g., biofilm-material interactions. In this study, the material properties appeared to influence the measured bacterial properties depending on the assay used. These approaches could provide a clearer image of bacterial growth where previous results may have been contradictory.

Three different latex blends (30%, 50%, and 60% PS) yielding interesting responses in terms of biofilm viability and PNAG abundances were used in further proteomic studies. Differences in protein expression and abundance profiles were observed both between the growth assays and among surfaces. Hence, the choice of the biofilm-forming assay affected both the number of proteins identified and the abundance profiles. Compared to the WP-based assay, the AP-based assay was better suited to detect substrate-induced differences in the surface expression of virulence-associated proteins. Although all the proteins identified in this assay were also detected in the WP-based assay, the abundance profiles of the biofilms were distinguished among material surfaces. Importantly, a subset of virulence-related proteins of the *S. aureus* surfaceome was identified to respond to the topographical features of the substrates, thus showing a strong correlation (Pearson's $r \geq |0.8|$) with surface roughness parameters. In the AP-based

assay 20/26 investigated proteins correlated with at least one roughness parameter, whereas in the WP-based assay 28/31 investigated proteins correlated with some roughness parameter. Furthermore, while parameters describing fine structure recurred as correlating parameters in the AP-based assay, the peak height and dominance as well as distance between asperities could commonly be correlated to protein abundances in the WP-based assay.

The results highlight the complexity of the *S. aureus* response to the topography of their environment, while additionally indicating a potential difference in pathogenicity depending on the biofilm growth assay. These findings provide new approaches for discovering, modelling and developing novel functional surfaces that limit bacterial growth and/or PNAG content as well as pathogenicity.

Data availability

All data analysed during this study are included in this published article or in its supplementary information file. Complementary data of these findings are available from the corresponding authors upon reasonable request.

CRediT authorship contribution statement

Paola San-Martin-Galindo: Conceptualisation, Methodology, Formal analysis, Investigation, Resources, Data curation, Visualization, Writing - original draft, Writing - review & editing. **Emil Rosqvist:** Conceptualisation, Methodology, Formal analysis, Investigation, Resources, Data curation, Visualisation, Writing - original draft, Writing - review & editing. **Stiina Tolvanen:** Methodology, Investigation, Resources, Writing - review & editing. **Ilkka Miettinen:** Formal analysis, Resources, Data curation, Visualisation, Writing - review & editing. **Kirsi Savijoki:** Methodology, Formal analysis, Resources, Writing - review & editing. **Tuula A. Nyman:** Formal analysis, Data curation, Visualisation, Writing - review & editing. **Adyary Fallarero:** Conceptualisation, Methodology, Writing - review & editing, Supervision, Funding acquisition. **Jouko Peltonen:** Conceptualisation, Methodology, Writing - review & editing, Supervision, Funding acquisition.

Declaration of Competing Interest

The authors declare that they have no known competing financial interests or personal relationships that could have appeared to influence the work reported in this paper.

Acknowledgements

The authors are grateful for the financial support received from the Academy of Finland (Decision N° 307466), the Jane and Aatos Erkko Foundation (Project: ABC Health), as well as personal grants from Waldemar von Frenckells Stiftelse, Svenska Kulturfonden and Åbo Akademi University.

Appendix A. Supplementary material

Supplementary data to this article can be found online at https://doi.org/10.1016/j.matdes.2021.109879.

References

[1] H.H. Tuson, D.B. Weibel, Bacteria–surface interactions, Soft Matter 9 (2013) 4368–4380, https://doi.org/10.1039/C3SM27705D.
[2] H.-C. Flemming, J. Wingender, U. Szewzyk, P. Steinberg, S.A. Rice, S. Kjelleberg, Biofilms: an emergent form of bacterial life, Nat. Rev. Microbiol. 14 (2016) 563–575, https://doi.org/10.1038/nrmicro.2016.94.
[3] M. Otto, Staphylococcal infections: mechanisms of biofilm maturation and detachment as critical determinants of pathogenicity, Annu. Rev. Med. 64 (2013) 175–188, https://doi.org/10.1146/annurev-med-042711-140023.
[4] J.W. Costerton, P.S. Stewart, E.P. Greenberg, Bacterial biofilms: a common cause of persistent infections, Science 284 (1999) 1318–1322, https://doi.org/10.1126/science.284.5418.1318.
[5] R.M. Donlan, Biofilms: microbial life on surfaces, Emerg. Infect. Dis. 8 (2002) 881–890, https://doi.org/10.3201/eid0809.020063.
[6] M. Toyofuku, T. Inaba, T. Kiyokawa, N. Obana, Y. Yawata, N. Nomura, Environmental factors that shape biofilm formation, Biosci. Biotechnol. Biochem. 80 (2016) 7–12, https://doi.org/10.1080/09168451.2015.1058701.
[7] J. Yan, B.L. Bassler, Surviving as a community: antibiotic tolerance and persistence in bacterial biofilms, Cell Host Microbe. 26 (2019) 15–21, https://doi.org/10.1016/j.chom.2019.06.002.
[8] Y. Cheng, G. Feng, C.I. Moraru, Micro- and nanotopography sensitive bacterial attachment mechanisms: a review, Front. Microbiol. 10 (2019) 191, https://doi.org/10.3389/fmicb.2019.00191.
[9] V. Carniello, B.W. Peterson, H.C. van der Mei, H.J. Busscher, Physico-chemistry from initial bacterial adhesion to surface-programmed biofilm growth, Adv. Colloid Interface Sci. 261 (2018) 1–14, https://doi.org/10.1016/j.cis.2018.10.005.
[10] M. Otto, Staphylococci in the human microbiome: the role of host and interbacterial interactions, Curr. Opin. Microbiol. 53 (2020) 71–77, https://doi.org/10.1016/j.mib.2020.03.003.
[11] J.S. Kavanaugh, A.R. Horswill, Impact of environmental cues on staphylococcal quorum sensing and biofilm development, J. Biol. Chem. 291 (2016) 12556–12564, https://doi.org/10.1074/jbc.R116.722710.
[12] H. Rohde, E.C. Burandt, N. Siemssen, L. Frommelt, C. Burdelski, S. Wurster, S. Scherpe, A.P. Davies, L.G. Harris, M.A. Horstkotte, J.K.-M. Knobloch, C. Ragunath, J.B. Kaplan, D. Mack, Polysaccharide intercellular adhesin or protein factors in biofilm accumulation of *Staphylococcus epidermidis* and *Staphylococcus aureus* isolated from prosthetic hip and knee joint infections, Biomaterials 28 (2007) 1711–1720, https://doi.org/10.1016/j.biomaterials.2006.11.046.
[13] E.J. Stewart, M. Ganesan, J.G. Younger, M.J. Solomon, Artificial biofilms establish the role of matrix interactions in staphylococcal biofilm assembly and disassembly, Sci. Rep. 5 (2015) 13081, https://doi.org/10.1038/srep13081.
[14] M.H. Lin, J.C. Shu, L.P. Lin, K. yu Chong, Y.W. Cheng, J.F. Du, S.-T. Liu, Elucidating the Crucial Role of Poly N-Acetylglucosamine from Staphylococcus aureus in Cellular Adhesion and Pathogenesis, PLOS ONE. 10 (2015) e0124216. https://doi.org/10.1371/journal.pone.0124216.
[15] T.J. Foster, J.A. Geoghegan, V.K. Ganesh, M. Höök, Adhesion, invasion and evasion: the many functions of the surface proteins of *Staphylococcus aureus*, Nat. Rev. Microbiol. 12 (2014) 49–62, https://doi.org/10.1038/nrmicro3161.
[16] S.R. Clarke, S.J. Foster, Surface adhesins of *Staphylococcus aureus*, Adv. Microb. Physiol. 51 (2006) 187–224, https://doi.org/10.1016/S0065-2911(06)51004-5.
[17] S. Ostvar, B. Wood, Multiscale model describing bacterial adhesion and detachment, Langmuir 32 (2016), https://doi.org/10.1021/acs.langmuir.6b00882.
[18] S.D. Puckett, E. Taylor, T. Raimondo, T.J. Webster, The relationship between the nanostructure of titanium surfaces and bacterial attachment, Biomaterials 31 (2010) 706–713, https://doi.org/10.1016/j.biomaterials.2009.09.081.
[19] Q. Xue, X.-B. Liu, Y.-H. Lao, L.-P. Wu, D. Wang, Z.-Q. Zuo, J.-Y. Chen, J. Hou, Y.-Y. Bei, X.-F. Wu, K.W. Leong, H. Xiang, J. Han, Anti-infective biomaterials with surface-decorated tachyplesin I, Biomaterials 178 (2018) 351–362, https://doi.org/10.1016/j.biomaterials.2018.05.008.
[20] J.K. Oh, Y. Yegin, F. Yang, M. Zhang, J. Li, S. Huang, S.V. Verkhoturov, E.A. Schweikert, K. Perez-Lewis, E.A. Scholar, T.M. Taylor, A. Castillo, L. Cisneros-Zevallos, Y. Min, M. Akbulut, The influence of surface chemistry on the kinetics and thermodynamics of bacterial adhesion, Sci. Rep. 8 (2018) 17247, https://doi.org/10.1038/s41598-018-35343-1.
[21] E.P. Ivanova, V.K. Truong, J.Y. Wang, C.C. Berndt, R.T. Jones, I.I. Yusuf, I. Peake, H.W. Schmidt, C. Fluke, D. Barnes, R.J. Crawford, Impact of nanoscale roughness of titanium thin film surfaces on bacterial retention, Langmuir ACS J. Surf. Colloids. 26 (2010) 1973–1982, https://doi.org/10.1021/la902623c.
[22] Y. Luan, S. Liu, M. Pihl, H.C. [van der Mei, J. Liu, F. Hizal, C.-H. Choi, H. Chen, Y. Ren, H.J. Busscher, Bacterial interactions with nanostructured surfaces, Curr. Opin. Colloid Interface Sci. 38 (2018) 170–189. https://doi.org/10.1016/j.cocis.2018.10.007.
[23] R.J. Crawford, H.K. Webb, V.K. Truong, J. Hasan, E.P. Ivanova, Surface topographical factors influencing bacterial attachment, Adv. Colloid Interface Sci. 179–182 (2012) 142–149, https://doi.org/10.1016/j.cis.2012.06.015.
[24] R. Bos, H.C. van der Mei, H.J. Busscher, Physico-chemistry of initial microbial adhesive interactions – its mechanisms and methods for study, FEMS Microbiol. Rev. 23 (1999) 179–230, https://doi.org/10.1111/j.1574-6976.1999.tb00396.x.
[25] B. Jansen, W. Kohnen, Prevention of biofilm formation by polymer modification, J. Ind. Microbiol. 15 (1995) 391–396, https://doi.org/10.1007/bf01569996.
[26] V.K. Truong, R. Lapovok, Y.S. Estrin, S. Rundell, J.Y. Wang, C.J. Fluke, R.J. Crawford, E.P. Ivanova, The influence of nano-scale surface roughness on bacterial adhesion to ultrafine-grained titanium, Biomaterials 31 (2010) 3674–3683, https://doi.org/10.1016/j.biomaterials.2010.01.071.
[27] F. Alam, K. Balani, Adhesion force of *Staphylococcus aureus* on various biomaterial surfaces, J. Mech. Behav. Biomed. Mater. 65 (2017) 872–880, https://doi.org/10.1016/j.jmbbm.2016.10.009.
[28] K.A. Whitehead, J. Colligon, J. Verran, Retention of microbial cells in substratum surface features of micrometer and sub-micrometer dimensions,

Colloids Surf. B Biointerfaces. 41 (2005) 129–138, https://doi.org/10.1016/j.colsurfb.2004.11.010.
[29] K. Bazaka, R.J. Crawford, E.P. Ivanova, Do bacteria differentiate between degrees of nanoscale surface roughness?, Biotechnol. J. 6 (2011) 1103–1114, https://doi.org/10.1002/biot.201100027.
[30] F. Aykent, I. Yondem, A.G. Ozyesil, S.K. Gunal, M.C. Avunduk, S. Ozkan, Effect of different finishing techniques for restorative materials on surface roughness and bacterial adhesion, J. Prosthet. Dent. 103 (2010) 221–227, https://doi.org/10.1016/S0022-3913(10)60034-0.
[31] B. Li, B.E. Logan, Bacterial adhesion to glass and metal-oxide surfaces, Colloids Surf. B Biointerfaces. 36 (2004) 81–90, https://doi.org/10.1016/j.colsurfb.2004.05.006.
[32] E. Rosqvist, E. Niemelä, A.P. Venu, R. Kummala, P. Ihalainen, M. Toivakka, J.E. Eriksson, J. Peltonen, Human dermal fibroblast proliferation controlled by surface roughness of two-component nanostructured latex polymer coatings, Colloids Surf. B Biointerfaces. 174 (2019) 136–144, https://doi.org/10.1016/j.colsurfb.2018.10.064.
[33] H. Juvonen, A. Määttänen, P. Laurén, P. Ihalainen, A. Urtti, M. Yliperttula, J. Peltonen, Biocompatibility of printed paper-based arrays for 2-D cell cultures, Acta Biomater. 9 (2013) 6704–6710, https://doi.org/10.1016/j.actbio.2013.01.033.
[34] H. Juvonen, T. Oja, A. Määttänen, J. Sarfraz, E. Rosqvist, T.A. Riihimäki, M. Toivakka, M. Kulomaa, P. Vuorela, A. Fallarero, J. Peltonen, P. Ihalainen, Protein and bacterial interactions with nanostructured polymer coatings, Colloids Surf. B Biointerfaces. 136 (2015) 527–535, https://doi.org/10.1016/j.colsurfb.2015.09.061.
[35] E. Rosqvist, E. Niemelä, J. Frisk, H. Öblom, R. Koppolu, H. Abdelkader, D. Soto Véliz, M. Mennillo, A.P. Venu, P. Ihalainen, M. Aubert, N. Sandler, C.-E. Wilén, M. Toivakka, J.E. Eriksson, R. Österbacka, J. Peltonen, A low-cost paper-based platform for fast and reliable screening of cellular interactions with materials, J Mater Chem B. 8 (2020) 1146–1156, https://doi.org/10.1039/C9TB01958H.
[36] R.N. Wenzel, Resistance of solid surfaces to wetting by water, Ind. Eng. Chem. 28 (1936) 988–994, https://doi.org/10.1021/ie50320a024.
[37] J. Peltonen, M. Järn, S. Areva, M. Linden, J.B. Rosenholm, Topographical parameters for specifying a three-dimensional surface, Langmuir 20 (2004) 9428–9431, https://doi.org/10.1021/la0400252.
[38] C.J. van Oss, Use of the combined Lifshitz–van der Waals and Lewis acid–base approaches in determining the apolar and polar contributions to surface and interfacial tensions and free energies, J. Adhes. Sci. Technol. 16 (2002) 669–677, https://doi.org/10.1163/156856102760099870.
[39] H. Juvonen, A. Määttänen, P. Ihalainen, T. Viitala, J. Sarfraz, J. Peltonen, Enhanced protein adsorption and patterning on nanostructured latex-coated paper, Colloids Surf. B Biointerfaces. 118 (2014) 261–269, https://doi.org/10.1016/j.colsurfb.2014.03.050.
[40] A.K. Hiltunen, P.M. Vuorela, A. Fallarero, Bisphosphonates offer protection against prosthetic joint infections caused by *Staphylococcus aureus* and *Staphylococcus epidermidis* biofilms, J. Drug Deliv. Sci. Technol. 40 (2017) 136–141, https://doi.org/10.1016/j.jddst.2017.06.002.
[41] M.E. Skogman, P.M. Vuorela, A. Fallarero, Combining biofilm matrix measurements with biomass and viability assays in susceptibility assessments of antimicrobials against *Staphylococcus aureus* biofilms, J. Antibiot. (Tokyo) 65 (2012) 453–459, https://doi.org/10.1038/ja.2012.49.
[42] A.K. Hiltunen, K. Savijoki, T.A. Nyman, I. Miettinen, P. Ihalainen, J. Peltonen, A. Fallarero, Structural and functional dynamics of *Staphylococcus aureus* biofilms and biofilm matrix proteins on different clinical materials, Microorganisms. 7 (2019), https://doi.org/10.3390/microorganisms7120584.
[43] K. Savijoki, I. Miettinen, T.A. Nyman, M. Kortesoja, L. Hanski, P. Varmanen, A. Fallarero, Growth mode and physiological state of cells prior to biofilm formation affect immune evasion and persistence of *Staphylococcus aureus*, Microorganisms. 8 (2020), https://doi.org/10.3390/microorganisms8010106.
[44] M.B. Lorey, K. Rossi, K.K. Eklund, T.A. Nyman, S. Matikainen, Global characterization of protein secretion from human macrophages following non-canonical caspase-4/5 inflammasome activation, Mol. Cell. Proteomics MCP. 16 (2017) S187–S199, https://doi.org/10.1074/mcp.M116.064840.
[45] E.W. Deutsch, A. Csordas, Z. Sun, A. Jarnuczak, Y. Perez-Riverol, T. Ternent, D.S. Campbell, M. Bernal-Llinares, S. Okuda, S. Kawano, R.L. Moritz, J.J. Carver, M. Wang, Y. Ishihama, N. Bandeira, H. Hermjakob, J.A. Vizcaíno, The ProteomeXchange consortium in 2017: supporting the cultural change in proteomics public data deposition, Nucleic Acids Res. 45 (2017) D1100–D1106. https://doi.org/10.1093/nar/gkw936.
[46] B. Pitts, A. Willse, G.A. McFeters, M.A. Hamilton, N. Zelver, P.S. Stewart, A repeatable laboratory method for testing the efficacy of biocides against toilet bowl biofilms, J. Appl. Microbiol. 91 (2001) 110–117, https://doi.org/10.1046/j.1365-2672.2001.01342.x.
[47] D. Szklarczyk, A.L. Gable, D. Lyon, A. Junge, S. Wyder, J. Huerta-Cepas, M. Simonovic, N.T. Doncheva, J.H. Morris, P. Bork, L.J. Jensen, C. von Mering, STRING v11: protein-protein association networks with increased coverage, supporting functional discovery in genome-wide experimental datasets, Nucleic Acids Res. 47 (2019) D607–D613, https://doi.org/10.1093/nar/gky1131.
[48] M. Ashburner, C.A. Ball, J.A. Blake, D. Botstein, H. Butler, J.M. Cherry, A.P. Davis, K. Dolinski, S.S. Dwight, J.T. Eppig, M.A. Harris, D.P. Hill, L. Issel-Tarver, A. Kasarskis, S. Lewis, J.C. Matese, J.E. Richardson, M. Ringwald, G.M. Rubin, G. Sherlock, Gene Ontology: tool for the unification of biology, Nat. Genet. 25 (2000) 25–29, https://doi.org/10.1038/75556.
[49] J.J. Almagro Armenteros, K.D. Tsirigos, C.K. Sønderby, T.N. Petersen, O. Winther, S. Brunak, G. von Heijne, H. Nielsen, SignalP 5.0 improves signal peptide predictions using deep neural networks, Nat. Biotechnol. 37 (2019) 420–423, https://doi.org/10.1038/s41587-019-0036-z.
[50] L.D. Renner, D.B. Weibel, Physicochemical regulation of biofilm formation, MRS Bull. 36 (2011) 347–355, https://doi.org/10.1557/mrs.2011.65.
[51] E.F. Haney, M.J. Trimble, J.T. Cheng, Q. Vallé, R.E.W. Hancock, Critical assessment of methods to quantify biofilm growth and evaluate antibiofilm activity of host defence peptides, Biomolecules 8 (2018), https://doi.org/10.3390/biom8020029.
[52] M. Böl, A.E. Ehret, A. Bolea Albero, J. Hellriegel, R. Krull, Recent advances in mechanical characterisation of biofilm and their significance for material modelling, Crit. Rev. Biotechnol. 33 (2013) 145–171, https://doi.org/10.3109/07388551.2012.679250.
[53] T. Coenye, H.J. Nelis, *In vitro* and *in vivo* model systems to study microbial biofilm formation, J. Microbiol. Methods. 83 (2010) 89–105, https://doi.org/10.1016/j.mimet.2010.08.018.
[54] J.H. Merritt, D.E. Kadouri, G.A. O'Toole, Growing and analyzing static biofilms, Curr. Protoc. Microbiol. Chapter 1 (2005), https://doi.org/10.1002/9780471729259.mc01b01s00. Unit 1B.1.
[55] K. De Prijck, H. Nelis, T. Coenye, Efficacy of silver-releasing rubber for the prevention of *Pseudomonas aeruginosa* biofilm formation in water, Biofouling. 23 (2007) 405–411, https://doi.org/10.1080/08927010701647861.
[56] T. Oja, B. Blomqvist, K. Buckingham-Meyer, D. Goeres, P. Vuorela, A. Fallarero, Revisiting an agar-based plate method: What the static biofilm method can offer for biofilm research, J. Microbiol. Methods. 107 (2014), https://doi.org/10.1016/j.mimet.2014.10.008.
[57] L. Hsu, J. Fang, D.-A. Borca-Tasciuc, R. Worobo, C. Moraru, The effect of micro- and nanoscale topography on the adhesion of bacterial cells to solid surfaces, Appl. Environ. Microbiol. 79 (2013), https://doi.org/10.1128/AEM.03436-12.
[58] S. Chatterjee, N. Biswas, A. Datta, P.K. Maiti, Periodicities in the roughness and biofilm growth on glass substrate with etching time: Hydrofluoric acid etchant, PLoS ONE 14 (2019) 1–12, https://doi.org/10.1371/journal.pone.0214192.
[59] W.W. Navarre, O. Schneewind, Surface proteins of gram-positive bacteria and mechanisms of their targeting to the cell wall envelope, Microbiol. Mol. Biol. Rev. MMBR. 63 (1999) 174–229.
[60] W. Wang, C.J. Jeffery, An analysis of surface proteomics results reveals novel candidates for intracellular/surface moonlighting proteins in bacteria, Mol. Biosyst. 12 (2016) 1420–1431, https://doi.org/10.1039/c5mb00550g.
[61] L. Foulston, A.K.W. Elsholz, A.S. DeFrancesco, R. Losick, The extracellular matrix of *Staphylococcus aureus* biofilms comprises cytoplasmic proteins that associate with the cell surface in response to decreasing pH, MBio. 5 (2014) e01667–01614, https://doi.org/10.1128/mBio.01667-14.
[62] C.J. Jeffery, What is Protein Moonlighting and Why is it Important?, in: Moonlighting Proteins, John Wiley & Sons, Ltd, 2017: pp. 1–19. https://doi.org/10.1002/9781118951149.ch1.
[63] B. Henderson, A. Martin, Bacterial virulence in the moonlight: multitasking bacterial moonlighting proteins are virulence determinants in infectious disease, Infect. Immun. 79 (2011) 3476–3491, https://doi.org/10.1128/IAI.00179-11.
[64] M. Ibba, D. Soll, Aminoacyl-tRNA synthesis, Annu. Rev. Biochem. 69 (2000) 617–650, https://doi.org/10.1146/annurev.biochem.69.1.617.
[65] S. Fuchs, J. Pané-Farré, C. Kohler, M. Hecker, S. Engelmann, Anaerobic gene expression in *Staphylococcus aureus*, J. Bacteriol. 189 (2007) 4275–4289, https://doi.org/10.1128/JB.00081-07.
[66] N.H. Hajdamowicz, R.C. Hull, S.J. Foster, A.M. Condliffe, The impact of hypoxia on the host-pathogen interaction between neutrophils and *Staphylococcus aureus*, Int. J. Mol. Sci. 20 (2019), https://doi.org/10.3390/ijms20225561.
[67] A. Gründling, O. Schneewind, Synthesis of glycerol phosphate lipoteichoic acid in *Staphylococcus aureus*, Proc. Natl. Acad. Sci. U. S. A. 104 (2007) 8478–8483, https://doi.org/10.1073/pnas.0701821104.
[68] C. Jeffery, Intracellular proteins moonlighting as bacterial adhesion factors, AIMS Microbiol. 4 (2018) 362–376, https://doi.org/10.3934/microbiol.2018.2.362.
[69] A.C. Graf, A. Leonard, M. Schäuble, L.M. Rieckmann, J. Hoyer, S. Maass, M. Lalk, D. Becher, J. Pané-Farré, K. Riedel, Virulence factors produced by *Staphylococcus aureus* biofilms have a moonlighting function contributing to biofilm integrity, Mol. Cell. Proteomics MCP. 18 (2019) 1036–1053, https://doi.org/10.1074/mcp.RA118.001120.
[70] J. Purves, A. Cockayne, P.C.E. Moody, J.A. Morrissey, Comparison of the regulation, metabolic functions, and roles in virulence of the glyceraldehyde-3-phosphate dehydrogenase homologues gapA and gapB in *Staphylococcus aureus*, Infect. Immun. 78 (2010) 5223–5232, https://doi.org/10.1128/IAI.00762-10.
[71] M. Hammel, G. Sfyroera, D. Ricklin, P. Magotti, J.D. Lambris, B.V. Geisbrecht, A structural basis for complement inhibition by *Staphylococcus aureus*, Nat. Immunol. 8 (2007) 430–437, https://doi.org/10.1038/ni1450.
[72] M. Jusko, J. Potempa, T. Kantyka, E. Bielecka, H.K. Miller, M. Kalinska, G. Dubin, P. Garred, L.N. Shaw, A.M. Blom, Staphylococcal proteases aid in evasion of the human complement system, J. Innate Immun. 6 (2014) 31–46, https://doi.org/10.1159/000351458.
[73] B. Kreikemeyer, D. McDevitt, A. Podbielski, The role of the Map protein in *Staphylococcus aureus* matrix protein and eukaryotic cell adherence, Int. J. Med. Microbiol. 292 (2002) 283–295, https://doi.org/10.1078/1438-4221-00212.

[74] T.A. Łeski, A. Tomasz, Role of penicillin-binding protein 2 (PBP2) in the antibiotic susceptibility and cell wall cross-linking of *Staphylococcus aureus*: evidence for the cooperative functioning of PBP2, PBP4, and PBP2A, J. Bacteriol. 187 (2005) 1815–1824, https://doi.org/10.1128/JB.187.5.1815-1824.2005.
[75] P. Ebner, J. Rinker, F. Götz, Excretion of cytoplasmic proteins in *Staphylococcus* is most likely not due to cell lysis, Curr. Genet. 62 (2016) 19–23, https://doi.org/10.1007/s00294-015-0504-z.
[76] N. Allocati, M. Masulli, C. Di Ilio, V. De Laurenzi, Die for the community: an overview of programmed cell death in bacteria e1609, Cell Death Dis. 6 (2015) e1609, https://doi.org/10.1038/cddis.2014.570.
[77] E.-Y. Lee, D.-Y. Choi, D.-K. Kim, J.-W. Kim, J.O. Park, S. Kim, S.-H. Kim, D.M. Desiderio, Y.-K. Kim, K.-P. Kim, Y.S. Gho, Gram-positive bacteria produce membrane vesicles: proteomics-based characterization of *Staphylococcus aureus*-derived membrane vesicles, Proteomics 9 (2009) 5425–5436, https://doi.org/10.1002/pmic.200900338.